FINAL REPORT

CONTRACT NO [illegible]

STUDY OF FUNDAMENTAL REQUIREMENTS FOR HIGH BRIGHTNESS RAMAN LASER STUDIES

1 OCTOBER 1966 THROUGH 30 JUNE 1968

HUGHES

HUGHES AIRCRAFT C[illegible]PANY

HUGHES RESEARCH LABORATORIES • MALIBU

HUGHES RESEARCH LABORATORIES
Malibu, California

a division of hughes aircraft company

STUDY OF FUNDAMENTAL REQUIREMENTS FOR HIGH BRIGHTNESS RAMAN LASER STUDIES

Final Report
Contract No. NO 0014-67-C-0206
Order No. 306

1 October 1966 through 30 June 1968

F. J. McClung, Project Scientist
Quantum Physics Department

The research conducted under this contract is part of project DEFENDER under the joint sponsorship of the Advanced Research Projects Agency, the Office of Naval Research, and the Department of Defense.

LIST OF ILLUSTRATIONS

TABLE OF CONTENTS

ABSTRACT

We have studied stimulated Raman scattering (SRS) and nonlinear index effects in liquids composed of spherically symmetric molecules. We conclude that although SRS can be observed without self-focusing, nonlinear index effects, presumably because of molecular redistribution, are present and should lead to beam instabilities at somewhat higher powers.

We also have studied SRS in hydrogen gas pumped by a giant pulse ruby laser. We determined the stability conditions for various cell configurations and lengths. We designed and tested an H_2 Stokes oscillator which reliably produced up to 200 kW of Stokes power in a nearly diffraction-limited fundamental mode. An H_2 Stokes amplifier with over 30 dB small signal gain was built. While tests indicated that an amplifier output brightness of over 10^{16} W-cm^{-2} sr^{-1} could be obtained with the input provided by the H_2 Stokes oscillator, only 10^{14} W-cm^{-2} sr^{-1} was achieved because of difficulties in coupling the oscillator output into the amplifier. These difficulties resulted from the particular configuration used rather than any fundamental limitation.

Finally, we have made a theoretical study of the third order polarizability applied to hydrogen, and the resulting coupled Stokes-anti-Stokes waves. The study included steady state and transient behavior, as well as some possible explanations for the anomalous Stokes output from hydrogen gas.

BLANK PAGE

I. INTRODUCTION

In this program we have developed a prototype Raman oscillator-amplifier and demonstrated high brightness and brightness gain with moderate pump energies. We have shown that this prototype has the potential to achieve brightnesses in excess of 10^{16} W·cm^{-2} sr^{-1} with a 5 J ruby pump pulse, and have found no limits to further extensions. We feel that we were approaching the achievement of this brightness potential at the end of the contract period. The work accomplished can be conveniently divided into two major areas: (1) the search for strongly Raman-active liquids which are not subject to nonlinear index effects, particularly self-focusing; and (2) the use of gaseous hydrogen as a Raman medium.

The search for Raman-active liquids without nonlinear effects centered on those composed of spherically symmetric molecules. This work was reported in the Semiannual Technical Summary Report and is included below in Section II. Extensions of the theory reported in the Semiannual Technical Summary Report on the nonlinear index of symmetric-molecule liquids to general polarizations are given in Appendices I and II. This work led to the conclusion that although perhaps an order of magnitude improvement was to be found in nonlinear index effects by employing liquids with spherically symmetric molecules, these effects still placed an unsatisfactory limitation on the operation of a high brightness Raman device. The origin of these effects in spherically symmetric liquids is presumably the molecular redistribution phenomenon analyzed in Appendices I and II.[1]

The second area of work, covering the use of gaseous hydrogen as a Raman medium, is described in Section III. Nonlinear index effects in H_2 gas are negligibly small.[2] Preliminary work in H_2 gas used parallel-beam pumping and cells with nominally zero feedback to study Stokes output as a function of H_2 pressure and ruby laser pump intensity. The results of these experiments resemble those which would be expected if about 1% feedback existed, and show typical oscillator behavior[3]; however, there is no known mechanism which could provide this much feedback. There are other possible (but unlikely) origins of striking anomalous behavior which do not postulate any unknown mechanisms and which are consistent with observations to date; one of these is discussed in Section IV. However, further experiments would be required to verify these speculations. Aside from physics problems, our preliminary experiments gave useful information on the stability conditions for pumping a hydrogen amplifier cell.

Following the preliminary H_2 experiments, we built and tested a high brightness device consisting of a H_2 Stokes oscillator amplifier pumped by a giant-pulse ruby oscillator amplifier. A brightness gain

of 20 dB over the Stokes oscillator was obtained, giving a brightness of 10^{14} W-cm^{-2} sr^{-1}. Strongly saturated Stokes amplification was not achieved because of technical difficulties which could not be eliminated during the contract period. However, unlike other high brightness devices, the H_2 Stokes oscillator-amplifier has no obvious fundamental limitations on size and power output.

Section IV outlines the theory of the entire third-order polarizability which is the leading contributor to nonlinear effects in fluids. The Raman susceptibility and many other terms emerge. The coupled Stokes-anti-Stokes wave relations that result from employing this polarizability and a plane wave pump field in Maxwell's equations are reviewed. The magnitudes of the nonresonant nonlinear polarizability terms cannot be estimated from meager and uncertain Kerr data on H_2. Guessing a value, we demonstrate how the anomalous threshold behavior can be accounted for qualitatively. These non-Raman terms would not affect a well-designed high-brightness H_2 Raman amplifier, but they could affect the coherence of the low-output feeding oscillator.

II. EXPERIMENTS WITH SYMMETRIC MOLECULE LIQUIDS

We have conducted several experiments to study the SRS effect in liquids composed of spherically symmetric molecules. Careful measurements revealed no evidence of self-focusing in $SiBr_4$. However, with a multimode pump, we have observed evidence of a nonlinear index in the form of frequency spreading in the Stokes radiation. Threshold measurements for symmetric and nonsymmetric liquids, combined with cross section measurements, have provided a basis for comparison of theoretically predicted and observed gains.

A. Search for Self-Focusing in $SiBr_4$

Our initial observations of the laser and Raman radiation exiting from a 10 cm path length of $SiBr_4$ indicated some filamentary structure. However, careful control experiments showed that this was probably a result of a combination of weak higher order transverse modes in the GPL, and experimental difficulties encountered in imaging through the 2 m spectrograph. In order to obtain more conclusive results, we set up the apparatus to analyze the polarization of laser and Raman radiation, using circularly and linearly polarized pumps.[4] This technique has proved to be a very sensitive test for self-focusing in such liquids as nitrobenzene.[4] The radiation exiting from the cell is analyzed for polarization and wavelength, and a pronounced depolarization of the radiation is observed to accompany the onset of self-focusing (SRS threshold) with a circularly polarized pump. We detected no depolarization in $SiBr_4$ with this apparatus, although the theory of self-focusing (regardless of the underlying mechanism) indicates that there should be strong depolarization if self-focusing occurs. This negative result held even far enough above threshold to achieve substantial conversion to Stokes power and to excite at least five orders of Stokes radiation. It should be noted that if a 1/2 mm diameter pump by beam was used, the Stokes radiation often appeared in a small filament about 40 to 50 μ in diameter. Presumably this results because of spatial narrowing of the Stokes caused by the variation of intensity across the pump beam, and it demonstrates the large gains achieved in this liquid. Because the spatial variation of the pump affects the gain exponentially, the amplified Stokes beam falls off more rapidly as a function of the radius than the pump beam. For example, if the pump beam is gaussian, the gain has the form $G = \exp(\alpha L)$, where $\alpha = \alpha_0 \exp(-r^2/r_0^2)$. The amplified Stokes wave, normalized to the on-axis amplitude, is then

$$S(r) = \exp[\alpha_0 L (\exp(-r^2/r_0^2) - 1)].$$

This function falls to 1/e at a radius r_1 such that

$$r_1^2/r_o^2 = -\ln(1 - 1/a_oL) .$$

Since $a_oL \simeq 10$ for our pump intensity in $SiBr_4$, $r_1/r_o \simeq 0.3$; a pump diameter $2r_o \simeq 0.2$ mm gives a beam size $2r_1$ of 50 μ. The pump beam is derived from a 1.5 mm aperture and a 40 cm focal length lens, and has structure of this size. A pump variation $a = a_o(1 - r^2/r_o^2)$ gives a similar reduction in beam size for $a_oL \simeq 10$.

B. Spectral Observations

Using the 2 m spectrograph, we measured a Stokes shift of 225 cm^{-1} in $SiBr_4$, giving a first Stokes wavelength of 705.3 mμ. This would be a symmetric, or "breathing," mode of vibration of the $SiBr_4$ molecule. With tetrabutyl tin (TBT), which should also show spherical symmetry, we observed a shift of 2920 cm^{-1}, corresponding to a Stokes wavelength of 871.1 mμ. This indicates that a C-H vibration has the lowest threshold in TBT. Because the higher order Stokes shifts in TBT fall outside the range of the instrument, only the first order Stokes radiation was observed in this material. With $SiBr_4$, up to six orders of Stokes radiation were observed.

Our giant pulse laser typically operates in several longitudinal modes. A Fabry-Perot interferogram typically shows two to four modes, with spacings of about 0.6 cm^{-1}. Other observations with the high dispersion grating of the 2 m spectrograph typically indicate two modes spaced by 0.6 to 0.7 cm^{-1}. There is usually a time modulation of the pulse, indicating other, more closely spaced modes, probably adjacent longitudinal modes of the laser cavity.

It has been well established that frequency broadening is observed in the Raman emission of liquids which self-focus when a multimode pump is used.[5,6] This results from a modulation of the nonlinear index at harmonics of the difference frequencies of the pump.[7] We have observed such broadening effects in $SiBr_4$ and TBT, with the amount of broadening increasing with increasing pump power above threshold, and also increasing with the Stokes order for $SiBr_4$. We have observed up to 8.5 mμ broadening in the fifth order Stokes radiation from $SiBr_4$ and up to 7.4 mμ broadening in the first Stokes radiation from TBT. This spreading of about 130 cm^{-1} is many times the laser mode spacing of about 0.7 cm^{-1}, indicating that there is modulation of a nonlinear index in these materials. However, at least in $SiBr_4$, this nonlinear index does not lead to depolarization of a circularly polarized pump, our best test for self-focusing.

C. Threshold Measurements

Another good indication of the presence of self-focusing is the theoretical comparison of predicted gains using the incident laser intensity with the minimum gain needed experimentally to observe Stokes radiation. For this purpose, we have made threshold measurements on several liquids. These will be compared with measured spontaneous Raman cross sections in Section II-D. For the threshold measurements, the GPL beam was incident on a 1.5 mm aperture. Following this, a 40 cm focal length lens weakly focused the pump beam in the 10 cm cell. A magnesium oxide screen behind the cell scattered the output radiation to calibrated Stokes and laser detectors. The Stokes detection system was capable of detecting about 1 W of Stokes power from the cell, except for $SiBr_4$, where the minimum detectable power was somewhat higher because of the filters used. With this arrangement the entire cell length was within the depth of focus of the 40 cm lens, so that the resulting beam (about 0.5 mm in diameter) was approximately a plane wave throughout the cell. The thresholds measured with this apparatus are given in Table I. The error limits indicate the scatter in the data, and do not include calibration and other systematic errors. However, these errors, which should be less than 20%, should not affect the relative thresholds. A linearly polarized pump beam was used for all of these measurements.

TABLE I

Measured Thresholds

Material	Threshold Power, MW
Silicon tetrabromide	0.29 ±0.02
Tetrabutyl tin	0.29 ±0.03
Nitrobenzene	0.050 ±0.005
Benzene	0.14 ±0.01
Carbon disulfide	0.024 ±0.002
Carbon tetrachloride	0.65 ±0.03

These powers should be multiplied by 500 to give the threshold intensity in MW/cm^2. The above results for nitrobenzene and benzene can be compared with Wang's results[8] by taking into account the different beam sizes and extrapolating his results to a 10 cm cell length. We must also take into account the fact that our beam is nongaussian in profile. We have measured a spot size in the focal plane of the 40 cm lens which is four times the diffraction limit for the 1.5 mm aperture used. Therefore, if we take a "characteristic transverse radius of curvature"[8] of the laser intensity of one quarter of the beam radius, we find a predicted threshold of 0.045 MW for nitrobenzene and 0.16 MW for benzene. Thus, our results for these two materials are in good agreement with Wang's results and the theory of self-focusing.

D. Cross Section Measurements

In this section we describe the peak normal Raman cross section measurements and compare the resulting theoretical gains with the above threshold measurements.

1. Discussion of Experiments and Data

The normal Raman scattering data were taken with a cw argon laser operating at 514.5 mμ and a double monochromator arrangement with photodetection. The relative cross sections of several liquids were measured and the absolute peak cross sections calculated using our previous result of 1.3 cm^{-2} cross section per unit volume per unit wavelength for nitrobenzene.[9] The results are given in Table II.

TABLE II

Raman Scattering Data

Liquid	Raman Line, cm^{-1}	Peak Cross Section, cm^{-2}	Gain, cm^{-1}/MW/cm^2
Nitrobenzene	1345	1.3	1.4 x 10^{-3}
Benzene	992	2.4	2.52
Carbon Tetrachloride	440	0.82	0.82
Tin Tetrachloride	370	2.9	2.54
Silicon Tetrabromide	225	5.8	4.23

Unfortunately, no spontaneous Raman lines were observed in TBT with this apparatus.

The accuracy of these measurements is not well known, but is judged to be about 30%. The major limiting factor is that the double monochromator used had an instrumental width of about 0.07 mμ, making it difficult to determine linewidths accurately.

2. Comparison of Theoretical Gain with Threshold Measurements

The largest initial intensity available for amplification in the Raman cell results from the quantum mechanical zero-point vibrations in the electromagnetic field and is of the order of 10^{-5} W/cm^2. For our beam, this represents 2×10^{-8} W power. Since our detection system was capable of detecting about 1 W of output power, the required gain is about 5×10^7. For a double pass through a 10 cm cell, this implies a gain of 0.88 cm^{-1}. Table III gives theoretical gains obtained by multiplying the above gains (cm^{-1}/MW/cm^2) by the threshold laser intensity observed experimentally. F is the factor required to increase the laser power to give a theoretical gain equal to the gain required experimentally for the observation of Stokes emission.

TABLE III

Theoretical Gains

Liquid	Theoretical Gain	F
Nitrobenzene	0.035 cm^{-1}	25
Benzene	0.076	5
Carbon tetrachloride	0.266	3.3
Silicon tetrabromide	0.515	1.4

With the many cumulative errors involved in this comparison, the results appear adequate to explain the observed SRS from $SiBr_4$ on the basis of purely exponential gain. The results for nitrobenzene are consistent with our earlier measurements,[9] and reaffirm the necessity of invoking the self focusing process to explain the observed SRS. The present results for benzene and carbon tetrachloride are not conclusive.

E. Conclusions

Our measurements and theoretical expectations indicate that even symmetric molecule liquids will not be usable at desired power densities without beam instabilities. The theory of Appendix II shows that the threshold power for the self-focusing instability in such liquids can be accurately inferred from dc Kerr effect measurements. The lowest Kerr constant known to us is that of tetrabutyl tin,[10] for which a threshold power for self-focusing of several megawatts is predicted.

III. EXPERIMENTS WITH RAMAN EFFECT IN HYDROGEN GAS

Our work with H_2 gas consisted of preliminary experiments to study the stability properties with our giant pulse ruby laser pump, followed by the construction and operation of a hydrogen Raman oscillator-amplifier designed to achieve a high brightness output.

A. Hydrogen Stability Experiments

We have performed a number of experiments with H_2 cells pumped by a parallel giant pulse ruby laser beam. These experiments typically show an oscillator type instability in the Stokes output as a function of pump intensity.[3] The objectives were to delineate the dependence of this behavior on H_2 pressure and the physical configuration of the apparatus. In particular, we sought to eliminate sources of feedback which could lead to the oscillator behavior.

In a 50 cm long H_2 cell with uncoated, nearly perpendicular windows, we did not detect Stokes emission (at a level of approximately 1 W) over a range of ~ 14 to 70 atm of H_2. The maximum single-pass gain calculated was exp (4). The gain $G = \exp(\beta IL)$ is calculated using the pressure-independent gain constant $\beta = 1.5 \times 10^{-3}$ cm/MW,[11] the measured length of the cell, and the observed laser pump power converted to pump intensity. The conversion factor depends on the degree of transverse mode control used. The actual power density of the laser beam at the location of the Raman cell was checked experimentally. A 0.17 mm diameter aperture was carefully scanned across the laser beam in steps of 0.20 mm, and the laser output power was compared with the power measured on the other side of the aperture. The transverse mode structure of the laser was monitored for each data point. The scan was made twice, once with moderately successful efforts at transverse mode control and once with no effort to control the transverse mode. The scatter in the data was quite severe for the non-mode-selected case, with noticeable modulation on the transmitted beam. The mode-selected data showed some scatter caused by variations in the effectiveness of the transverse mode control and a much smaller residual scatter. Systematic variations and variations which are not understood appeared in both cases, but were much less apparent in the mode-selected case. The full width at half maximum for the two cases (from the smoothed curves) were 1.3 ±0.2 mm and 2.9 ±0.5 mm. Both curves appeared gaussian in shape, although some asymmetries were evident. The relevant power density values were 12 ±1 MW/cm^2 per MW of power output and 3 ±1 MW/cm^2 per MW of power output. Typical power output values were 5 MW (mode-selected) and 10 MW (non-mode-selected). These then correspond to a power density of 60 MW/cm^2 (mode-selected) and 30 MW/cm^2 (non-mode-selected).

In a 90 cm long cell with uncoated, nearly perpendicular windows, we observed Stokes emission at a calculated gain of about exp (6). The Stokes power increased very rapidly with pump intensity, a characteristic of oscillator threshold. There was some indication of a lower threshold at the higher H_2 pressures, above 10 to 15 atm. This is in contrast to the strong dependence on pressure observed by other workers.[12, 13]

We attempted to reduce feedback by tilting the cell windows farther from alignment with the pump beam. A slight increase in threshold with this configuration led us to insert a dispersing prism between the pump laser and H_2 cell (with tilted windows) to block feedback of the Stokes radiation through the pump laser. There was no further increase in threshold.

The apparent effect of tilting the windows on the 90 cm cell led to the hypothesis of "diffraction feedback" from cell windows which are not far from alignment with the pump beam. In this effect, the diffraction from the 4% reflection of the spatially narrowed (see Section II-A) Stokes beam would provide the source of feedback leading to oscillator behavior. Calculations showed that under typical operating conditions this effect gave feedback within an order of magnitude of that required to explain the oscillator behavior. In order to check this hypothesis and to further define the stability criteria for our H_2 amplifier, we used a 150 cm long section of the amplifier cell in the same parallel pump beam configuration. The Brewster's angle windows on this cell would reduce the diffraction feedback by orders of magnitude. However, there was little effect on threshold, with detectable Stokes emission appearing at a calculated gain of about exp (7). Thus, while diffraction feedback appears to be a contributing factor, it is not dominant in producing the oscillator-like instability in our experiments.

The majority of our preliminary H_2 experiments were performed with the 150 cm long section of the amplifier cell. With a more sensitive Stokes detection system we were able to observe the spontaneous Raman scattering and check its proportionality to H_2 pressure. A plot of relative Stokes output power as a function of ruby laser pump power is shown in Fig. 1. The curves show a linear relationship fitted to the spontaneous scattering data and the calculated exponential behavior of the stimulated scattering, assuming a gain constant of 1.5×10^{-3} cm/MW and a pump laser intensity of 10 MW/cm^2 per MW of pump power. The actual relationship between pump power and intensity varied from shot to shot, from about 5 to 12 MW/cm^2 per MW, depending on the purity of the transverse mode, and resulted in the scatter of the experimental points. However, the data show that an exponential gain constant from 2 to 4 times larger than 1.5×10^{-3} cm/MW is required to give the observed dependence on laser power, if amplifier behavior (i.e., exponential buildup) is assumed. The more likely explanation is that Fig. 1 demonstrates the extremely rapid (faster than exponential) buildup of oscillator output slightly above threshold.

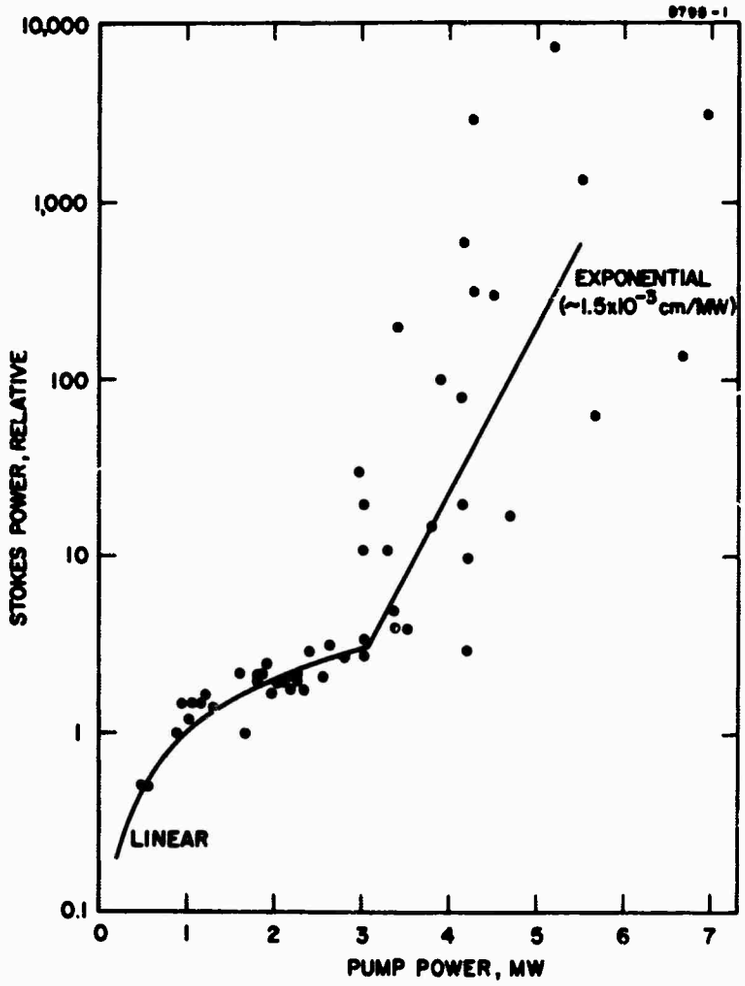

Fig. 1. A plot of relative Stokes output power from a 150 cm long H_2 cell as a function of pump power. Linear (spontaneous) and exponential (stimulated) regions are shown.

Similar measurements at 21.4, 7.8, and 5.1 atm pressure with a somewhat more reproducible brightness from the pump resulted in the following estimates of gain constants, assuming exponential buildup:

$$\beta_{21.4} = 3.8 \times 10^{-3} \text{ cm/MW}$$

$$\beta_{7.8} = 2.4 \times 10^{-3} \text{ cm/MW}$$

$$\beta_{5.1} = 2.6 \times 10^{-3} \text{ cm/MW} .$$

These values are estimated to be accurate within 50%. The apparent higher gain at 21.4 atm could be caused by the higher effective pulsed gain with larger Raman linewidth.[11] The output at a given pump level increases with increasing pressure, in agreement with the pressure dependence of the spontaneous scattering. Thus it does not appear that there is a large qualitative change in the Stokes scattering as the pressure is increased above about 10 atm.[12]

The following three conclusions can be drawn from these preliminary experiments: (1) the parallel beam-pumped geometry shows an oscillator-like instability; (2) there is a range of stable operation in the unsaturated amplification up to a total gain of approximately exp (6); and (3) this behavior is not strongly dependent on H_2 pressure.

B. Hydrogen Oscillator-Amplifier Experiments

Following our stability experiments we developed a hydrogen oscillator-amplifier arrangement, pumped by a ruby giant pulse oscillator-amplifier. The objective was to obtain a high brightness output from the amplifier by (1) using the output of a diffraction-limited, transverse mode-controlled H_2 Stokes oscillator as the amplifier input; and (2) operating the amplifier with strongly saturated gain. A small, relatively low output power oscillator can provide a high-quality output by the use of a high-Q cavity with some means of mode selection. The oscillator thus provides a high quality, large signal input to the amplifier. The amplifier operates in such a way that the effects of hot spots in the ruby pump beam are minimized, since the gain increases linearly with pump intensity rather than exponentially in the large signal case. With this arrangement, we have achieved 20 dB brightness gain in the amplifier, and an output brightness of 1×10^{14} W cm^{-2} sr^{-1}. Because of unanticipated difficulties encountered in coupling the H_2 oscillator output into the amplifier, we did not achieve strongly saturated amplification in the amplifier. This limited the brightness gain through both power gain and far field divergence angle. Our work has had the

following results: (1) it has demonstrated that this approach to obtaining high brightness is feasible; (2) it has shown the areas where further work is needed to optimize this approach; and (3) it has indicated how this device can be scaled up to obtain very high brightness.

In the following discussion we shall first describe the configuration and operating parameters of the apparatus, and then discuss in detail the characteristics of the H_2 oscillator and amplifier. Finally, we shall discuss the results, the improvements required for optimum operation, and the possibilities for scaling the device.

1. Apparatus

The apparatus is shown schematically in Fig. 2(a). A rotating prism, Q-switched ruby laser oscillator (shown in Fig. 2(b) and (c)) produces a 10 MW of power in a 40 nsec pulse. The output beam from this oscillator is enlarged to approximately 1 cm diameter by an afocal telescope and is then amplified in a 12 in. long by 5/8 in. diameter, Brewster angle ruby amplifier crystal (shown in Fig. 2(d)) pumped by up to 20 kJ of energy into four linear flashlamps. The output of the ruby amplifier is in excess of 200 MW and 6 J at full pump energy. Approximately 2 to 3% of this output is beam split off and used to pump the H_2 Stokes oscillator through a diaphragm aperture (not shown in Fig. 2) and a beam-reducing telescope which match the pump beam to the TEM_{00} mode of the H_2 oscillator cavity. The remainder of the ruby amplifier output is delayed by about 13 nsec and combined with the H_2 oscillator output at a dichroic mirror. The H_2 oscillator has a 50 cm long cavity formed by a 10 m radius mirror and a flat mirror. These mirrors reflect 99+% and 85%, respectively, at 0.975 μ, and transmit 85% and 70%, respectively, at 0.694 μ. The H_2 oscillator output appears in a beam of ~ 1 mm diameter, with a typical peak power of about 100 kW. This output beam is expanded in a 10-power afocal telescope to match the size of the ruby amplifier output beam, and the two beams are combined at a dichroic mirror. The combined beam is enlarged to about 2.5 cm diameter by a final afocal telescope and then enters the H_2 Stokes amplifier. The H_2 amplifier is 3 m long, with a clear aperture of about 3 cm. The cell has Brewster angle windows. The two H_2 cells are connected together and filled with pure H_2 gas at pressures up to 50 atm.

Detectors monitor the power output of the ruby amplifier and the power input and output of the H_2 amplifier. Calibration of these detectors is derived from an ITT FW 114A Bi Planar photodiode calibrated at 0.694 μ and from the relative response of the S-1 photosurface at 0.694 and 0.975 μ. The far field patterns at the H_2 amplifier input and output are photographed with a high quality 1.6 m focal length telescope. The brightness gain is measured by attenuating the H_2 amplifier output far-field monitor beam and comparing the observed far-field patterns of input and output.

D772-1

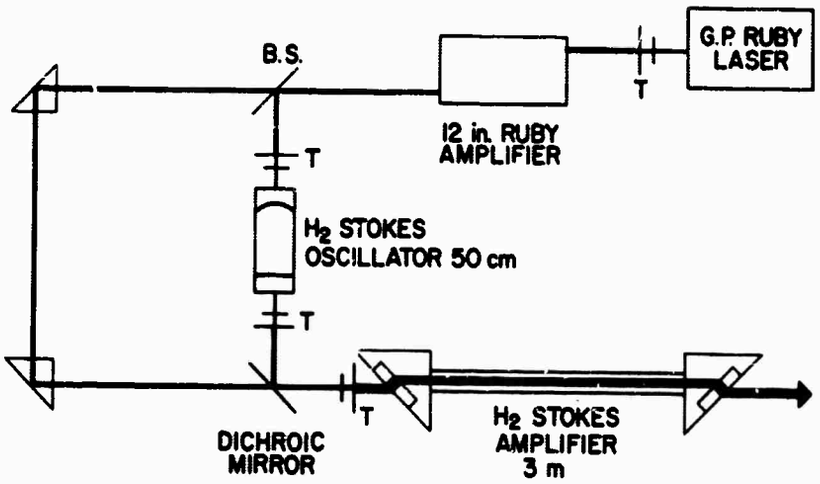

Fig. 2(a) Schematic diagram of giant pulse ruby laser oscillator-amplifier, hydrogen Stokes oscillator-amplifier apparatus.

M4787 D795-5

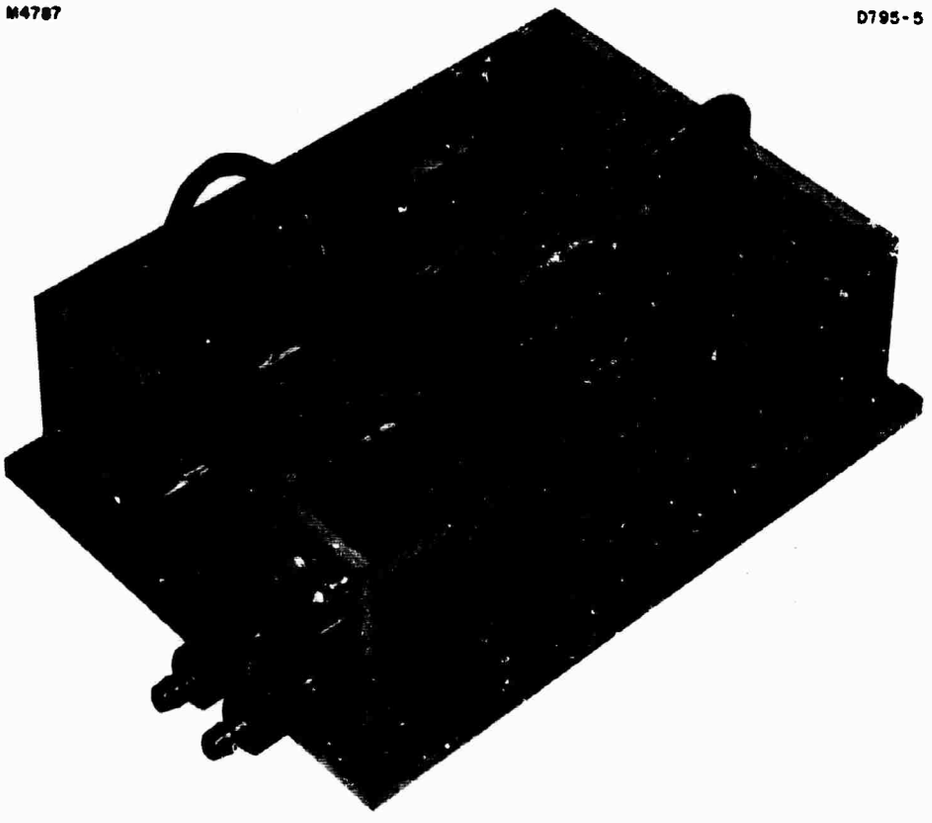

Fig. 2(b) Giant pulse ruby laser oscillator head.

M5146 D795-6

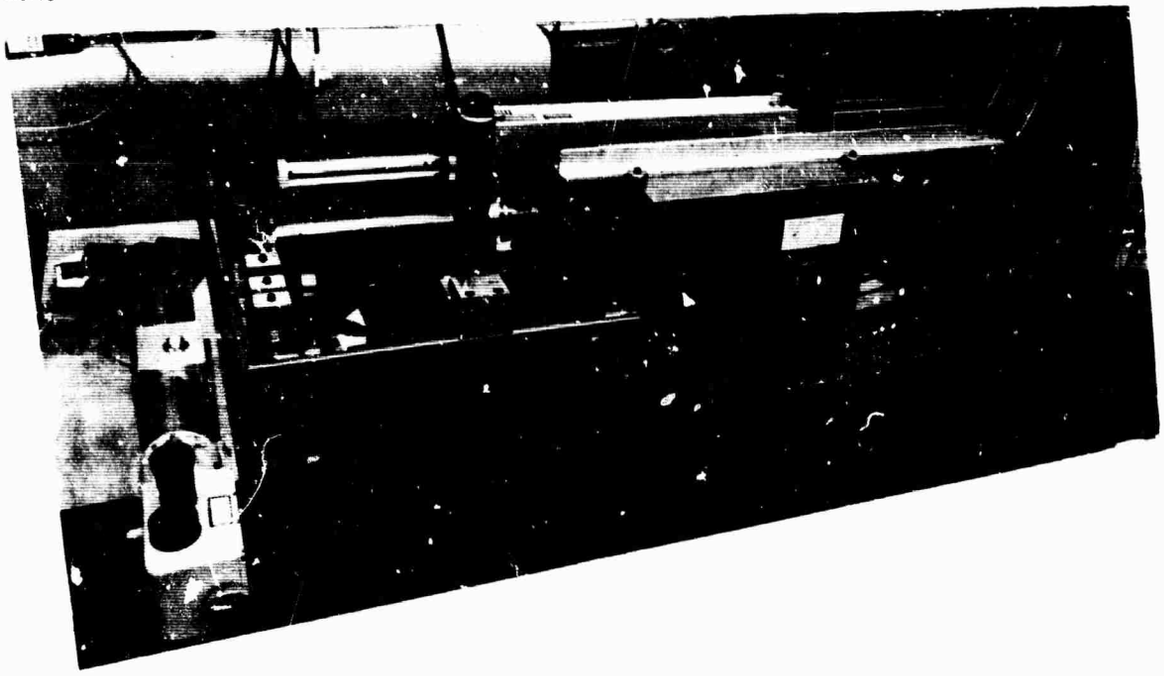

Fig. 2(c). Giant pulse ruby laser oscillator system.

M5641

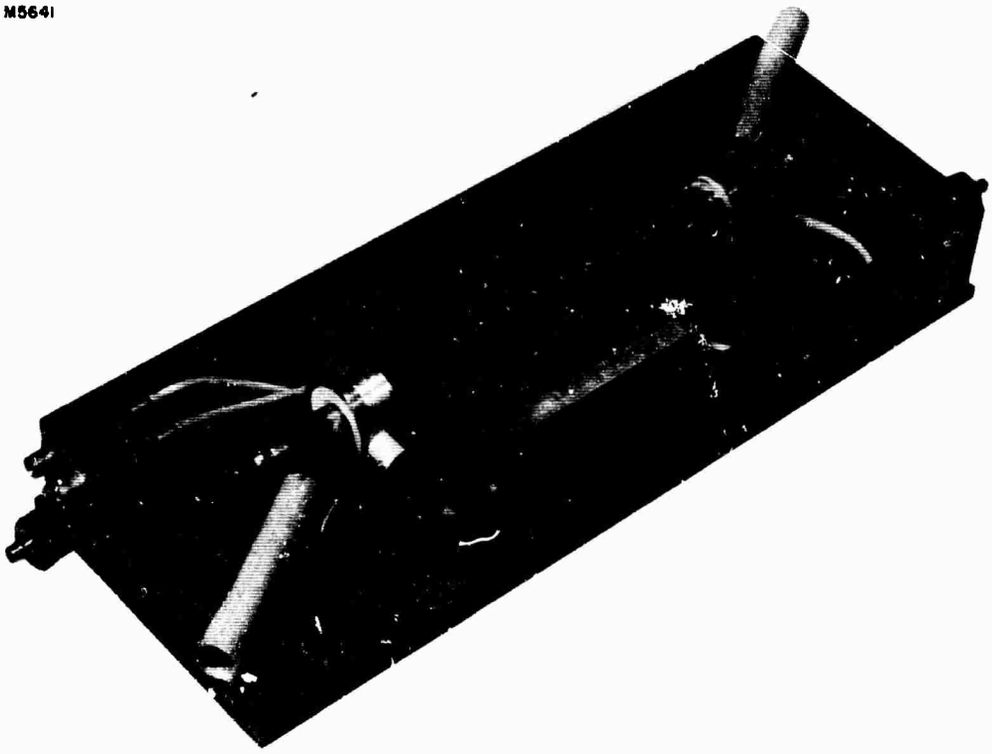

Fig. 2(d). Brewster angle ruby laser amplifier. Helical lamp shown with reflector removed. Linear lamp model not shown.

2. The Hydrogen Stokes Oscillator

The H_2 Stokes oscillator is the key element in this system. It should provide a diffraction-limited beam (TEM_{00} mode) with sufficient power to saturate the H_2 amplifier. If the amplifier has 30 dB small signal gain, an input of several tens of kilowatts is required to strongly saturate the ruby laser pump beam.

For transverse mode control in the oscillator we used a rather high Q cavity with well-defined modes,[14] and selected the fundamental (TEM_{00}) mode by carefully matching the ruby pump beam to that mode. The matching is obtained by an aperture and a beam-reducing telescope immediately preceding the oscillator cavity. The input size of the pump beam is varied by adjusting the power of the telescope and the size of the aperture. The output size of the pump beam is controlled primarily by adjusting the focus of the telescope and, to a lesser degree, by the aperture size and telescope power. Pump power is controlled by the aperture size and, if necessary, by attenuation. With proper adjustment, this pumping method selectively excited the TEM_{00} mode of the cavity.

If pressure broadening is dominant, the Stokes gain is independent of pressure, while the linewidth increases linearly with pressure.[12] If the pump intensity is large enough at a given pressure, the Stokes buildup rate is so fast that some Fourier components of the Stokes signal lie outside the Stokes linewidth, leading to reduced effective gain.[11] For normal Stokes Raman scattering (as in the forward direction, where coupling to anti-Stokes can be neglected), the peak power gain per second of a wave packet is $2\pi c\Delta\nu V$ where $\Delta\nu(cm^{-1})$ is the full width of the transition, c is the velocity of light, and

$$V = \frac{\sqrt{1 + 4G} - 1}{2} ;$$

here $2\pi c\Delta\nu G$ is the peak gain per second that the pump would produce if the linewidth were infinite (see eq. (31), Section IV). A plot of V/G, i.e., the ratio of effective to directly calculated gain, as a function of G (proportional to pump power) is shown in Fig. 3. The arrow shows the point at which the calculated power gain (cm^{-1}) equals the linewidth (cm^{-1}).

At pressures of approximately 20 atm we observed that the pump power required to reach oscillation threshold was much larger than that calculated using the known cavity losses and a gain constant of 1.5×10^{-3} cm/MW. This phenomenon can be explained by the effect described above. Thus, establishment of an oscillation within the time duration

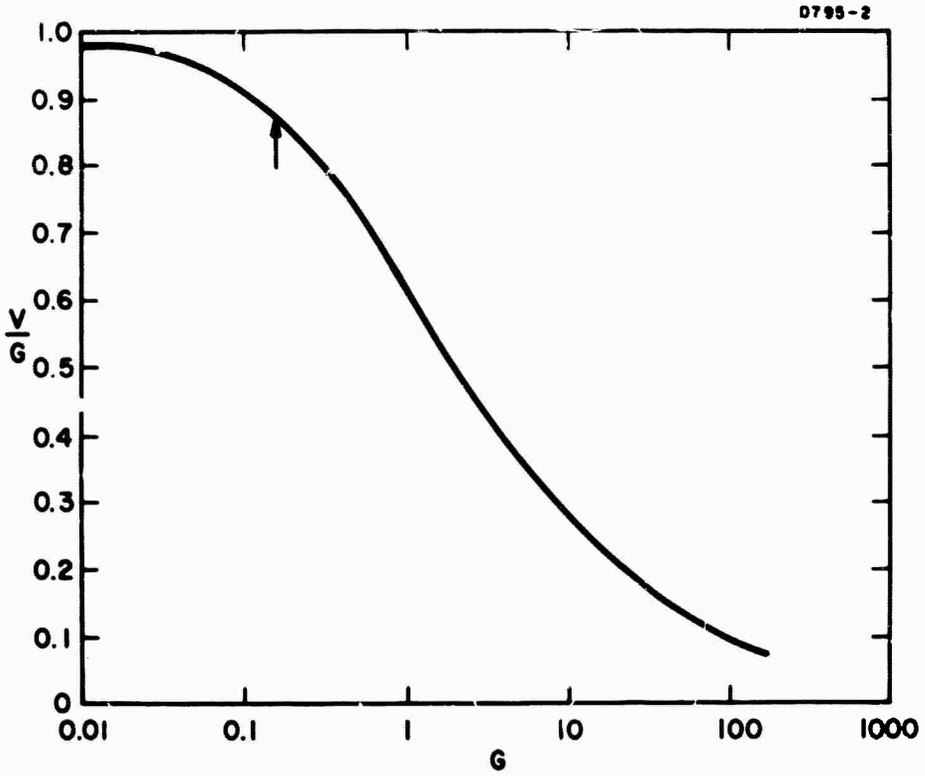

Fig. 3. A plot of the ratio of effective to directly calculated gain as a function of directly calculated gain (proportional to pump power). At the arrow, calculated gain equals line width.

of the pump pulse required excessively high pump powers at this pressure. We therefore studied the characteristics of the oscillator at several pressures up to 70 atm. We found that at ~50 atm we could obtain reliable Stokes output with the theoretically predicted threshold pump intensity.

The calculated passive mode diameter for our oscillator cavity is 1.6 mm (Ref. 14). However, we observed near-field patterns only about 1 mm in diameter. The far-field patterns also corresponded to a 1 mm beam. We believe that this effect results from the spatial variation of the gain in the cavity, i.e., the shape of the pump beam. These effects were first studied by Kogelnik[15] and extended to spherical-mirror cavities by Casperson and Yariv.[16] Calculations of the mode size to be expected with our operating parameters agree very well with our observations.[17]

A further effect resulting from the same phenomenon was also noticed: if the axis of the pump beam and the axis of the passive cavity are not collinear, the pump beam can geometrically "pull" the axis of the mode generated in the cavity away from the passive mode axis. This situation is shown schematically in Fig. 4, where the offset is caused by an angular alignment error α in the front reflector, leading to an offset $\Delta = \alpha R$ between the passive cavity mode and the pump beam. Note that the passive mode axis must always be a radius of the spherical mirror and must be normal to the flat mirror. If $\alpha = 3 \times 10^{-5}$ rad, then $\Delta = 0.3$ mm for the 10 m radius mirror we used. This is approximately our alignment accuracy, and gives an offset of one-third of the output beam diameter. Another cause of offsets is cylindrical distortion in the cavity mirrors caused by uneven distribution of the force on the mirrors over the mirror mounts; we have observed offsets of up to 3 mm from this cause. These distortions could be reduced to negligible values by careful adjustment of the mounts. Regardless of the cause of offsets, the spatial distribution of the pump causes the active cavity mode to form essentially along the pump axis because of the same physical process studied by Kogelnik[15] and by Casperson and Yariv.[16, 17] Because the cavity decay time is longer than the pump pulse length, much of the Stokes energy built up in the cavity while the pump is on decays after the pump shuts off. Furthermore, since the pulling effect disappears with the pump, this energy shifts to the passive cavity mode which is offset.

The more deleterious of these two effects is the reduction of the mode size, since in this case a higher power telescope must be used to provide the amplifier input. This in turn leads to more sensitivity to alignment errors, beam offsets, and chromatic aberrations in the lenses. For example, a 0.3 mm offset at the oscillator output, corresponding to our cavity alignment accuracy, gives a 7 mm offset at the amplifier,

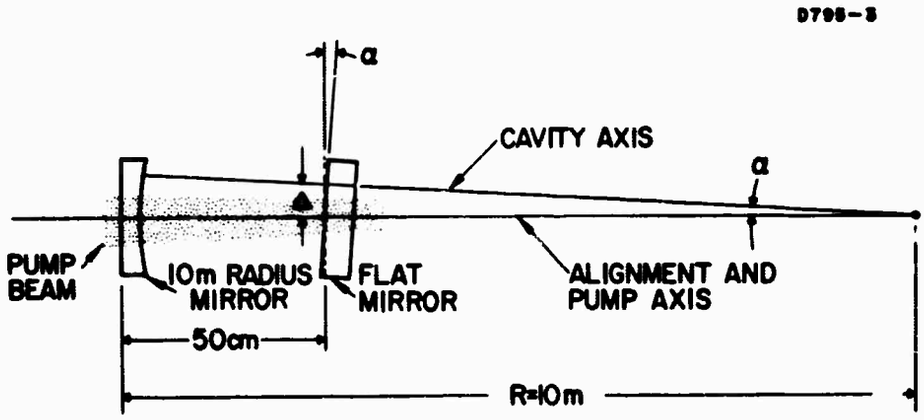

Fig. 4. Hydrogen Stokes oscillator configuration, showing mode offset generated by misalignment of the output mirror.

and additional errors exaggerate this result. The power generated during the pump pulse is pulled according to the above discussion, so that the offset is smaller. Even so, vignetting can occur fairly easily.

We have obtained considerable data on the performance of the oscillator. Much of this work used the giant pulse ruby laser oscillator directly as a pump, instead of the arrangement shown in Fig. 2. The only significant difference in the results is that the oscillator is somewhat more reliable when pumped directly by the GP oscillator. This apparently results primarily from the accumulation of optical damage to the beam splitter when the amplified ruby beam is used.

The evidence that a nearly diffraction limited (TEM_{00}) mode is generated in the H_2 oscillator includes beam divergence measurements and near-field patterns on Polaroid film. These data show that a beam of about 1 mm diameter is formed in the oscillator, reduced from the 1.6 mm passive mode size by the effects of the tightly coupled pump beam.[15-17] In addition, our experience has shown that threshold pump power, the time buildup and decay characteristics of the Stokes output, and the output modulation resulting from the beating of adjacent longitudinal modes of the cavity are all strongly correlated with the character of the transverse mode generated. A mode close to the desired TEM_{00} mode is associated with a lower threshold, slow buildup and decay with a single time constant, and a stable modulation. A poor mode usually occurs with a relatively high threshold, very rapid buildup, and faster decay, usually with two or three time constants apparently involved. As mentioned earlier, it was necessary to operate with H_2 pressures approaching 50 atm in order to achieve reliable generation of a good mode. Figure 5 shows some typical Stokes output data. Figure 5(a) shows about 125 kW peak Stokes power from a cavity formed by two flat mirrors with the same reflectivities as the mirrors otherwise used. (All other data are with the cavity shown in Fig. 2.) The decay is fairly rapid, with two distinct decay rates observed. Figure 5(b) and (c) show 160 kW and 100 kW peak powers, respectively, with rapid buildup and decay, and multiple decay rates. The modes associated with Fig. 5(a), (b), and (c) all had poor beam divergence. Figure 5(d) shows the output power associated with a good mode which had small beam divergence. Peak output power is 55 kW, and the pump power is only one-third to one-quarter of that required in the other parts of Fig. 5. Figure 6 shows the output associated with good modes on a more expanded time scale. Peak powers are about 50 kW. The slow buildup and smooth decay are evident, as well as the stable modulation resulting from mode beating. The decay rate agrees with that calculated from the cavity losses, and the modulation period equals the calculated cavity roundtrip transit time. The pressure is about 40 atm.

Another important feature in the H_2 oscillator is a time delay between the peak pump power and the peak Stokes output. Figures 7 and 8 show the ruby pump and Stokes output as measured by a single detector,

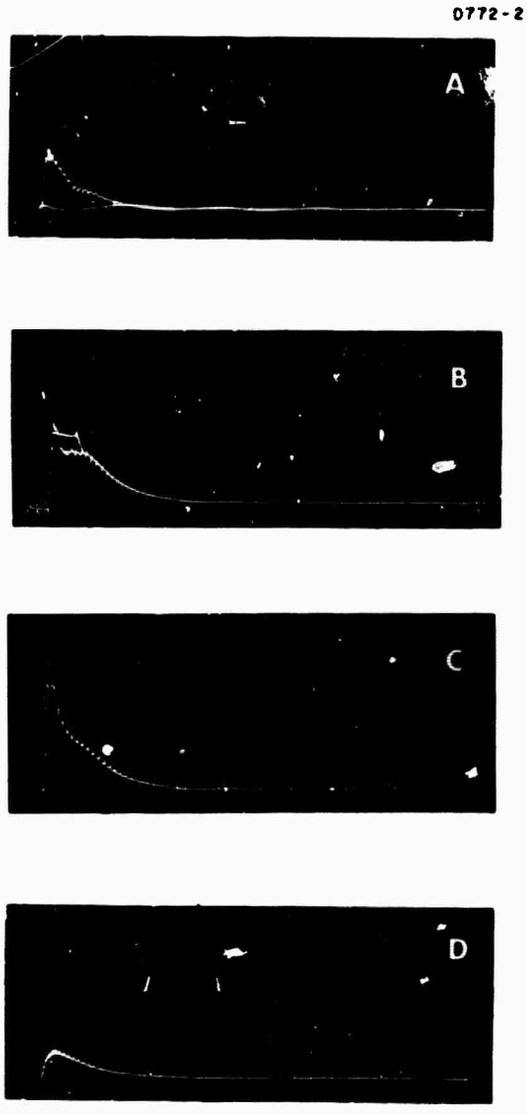

Fig. 5.
Hydrogen Stokes oscillator power output. Horizontal scale: 50 nsec/major div (see text).

D772-3

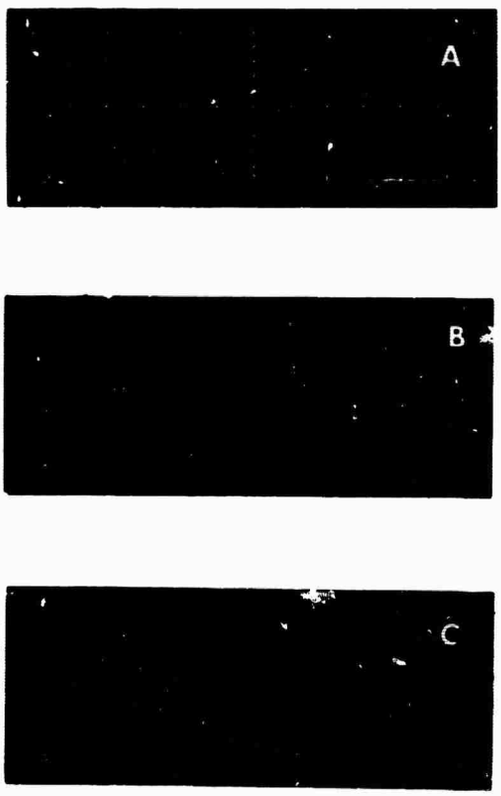

Fig. 6.
Hydrogen Stokes oscillator power output. Horizontal scale: 20 nsec/major div (see text).

D772-4

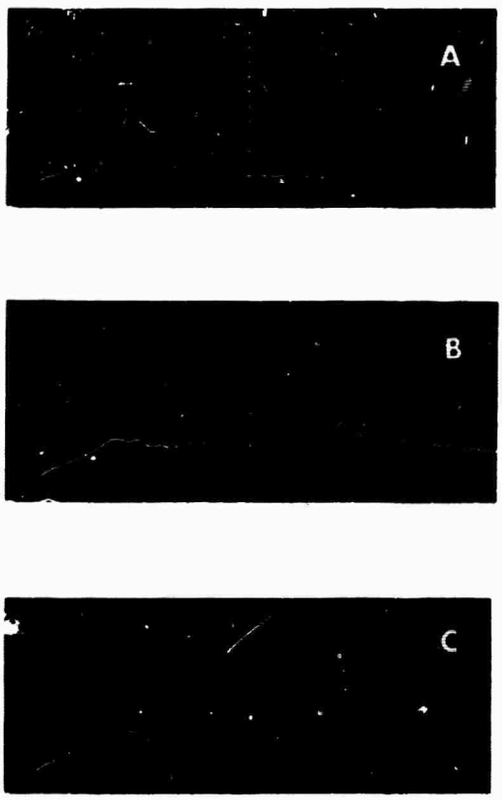

Fig. 7.
Hydrogen Stokes oscillator pump power and power output. Horizontal scale: 20 nsec/major div (see text).

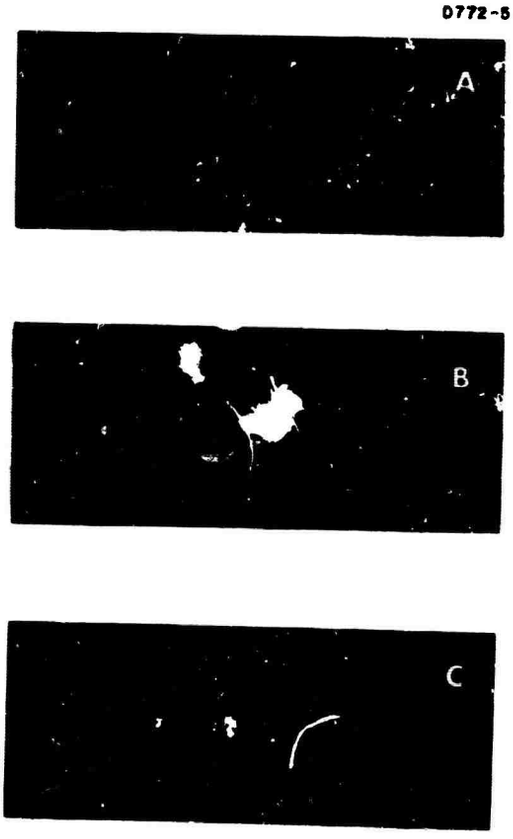

Fig. 8.
Hydrogen Stokes oscillator pump power and power output. Horizontal scale: 20 nsec/div (see text).

with sensitivity to the two wavelengths appropriately adjusted. The peak Stokes power in Fig. 8(c) is about 125 kW, and H_2 pressure is 48.5 atm. It is apparent that the time delay decreases as the oscillator is pumped further above threshold, reaching a minimum value of about 15 nsec. Near threshold, the oscillator must effectively integrate the entire pump pulse in order to build the spontaneous Stokes to an observable level, so that the delay time is on the order of the pump pulse width. Considerably above threshold, the gain per transit of the cavity is large, so that a fixed number of transits determines the time delay. Because the oscillator is normally operated considerably above threshold, an optical time delay of about 13 nsec was provided for the H_2 amplifier pump beam, so that the peak pump and signal powers would coincide in time.

We conclude that at H_2 pressures between 40 and 50 atm, this apparatus can produce greater than 100 kW Stokes power in a near diffraction limited 1 mm diameter fundamental mode with good reliability. Threshold, beam divergence, and time behavior of the output agree with expected characteristics, although the mode size is smaller than the calculated passive cavity mode size because of the spatial variation of the pump beam.

3. The Hydrogen Stokes Amplifier

The calculated unsaturated gain of the H_2 amplifier is $\exp(6.5)$, or 28 dB for 100 MW of input pump power, assuming a uniform distribution of the pump power over the aperture. The pump beam actually has some "hot spots" where the pump intensity is higher than the average. Since the unsaturated gain increases exponentially with pump intensity, these hot spots would lead to strong nonuniformities in the amplified beam and therefore increase the beam divergence of the output. This effect can be avoided to some degree by strongly saturating the amplifier as close to the input as possible. Operation at high signal levels also provides a higher conversion of pump to Stokes radiation.

We operated the H_2 amplifier over a wide range of pump levels with no input signal, in order to check its stability. The amplifier was stable throughout the expected operating range. Even with calculated gains of over 60 dB there was less than 5% conversion to Stokes power. These tests were made with the ruby amplifier output going directly into the H_2 amplifier.

With a dichroic mirror in place we first tested the system by eliminating the telescope following the H_2 oscillator but including the 2.5-power telescope preceding the amplifier. Thus we had a pump beam in the amplifier which was about 2.5 cm in diameter, while the signal beam was about 0.25 cm in diameter. We achieved brightness

gains of about 16 dB and output brightness in the range 0.4 to 1 x 10^{15} W - cm^{-2} sr^{-1}. With the 10-power telescope added, the signal beam diameter was increased to 2.5 cm. We observed brightness gains of about 20 dB and output brightness of about 1 x 10^{14} W - cm^{-2} sr^{-1}. The relatively small output brightness resulted because of a loss of input signal strength of about 13 dB. This loss will be discussed below. This meant that we were not able to reach high conversion efficiencies, nor could we take advantage of the relative smoothing effect of strong saturation in the amplifier.

The total available operating time with the system was rather severely limited by optical damage to the dichroic mirror. Four units were available, all of which had "hard" metal-metal oxide coatings. These coatings are more susceptible to giant pulse optical damage than some other types of coatings, particularly those developed specifically to withstand higher pulsed energies.

We have considered several possible causes for the large loss of Stokes signal. First, misalignment of one or both telescopes carrying the Stokes signal or alignment of the two telescopes to different axes could have caused vignetting of the beam. It should be noted that the alignment telescope used to align the system had to be reversed in its mount for the alignment of both telescopes; this involves some systematic error, which is small enough to be unimportant unless compounded by other errors. Second, our conception of the H_2 oscillator mode development as a function of time could be wrong, leading to a mismatch of beam sizes. This possibility cannot be completely eliminated without making time resolved studies of the modes; however, we have considerable data from the H_2 oscillator which we feel are consistent with our conception of its operation. This includes far-field patterns, near-field mode photographs and burn patterns, time resolved power output measurements, and correlation of these features with controlled misalignment of the oscillator cavity. Third, Stokes beam offsets can cause vignetting in the system. The two primary causes of these offsets are the mode shifting associated with misalignment, which was discussed above, and distortions of the pump beam as a result of optical damage at the beam splitter. We have observed offsets from both causes. As discussed earlier, the offset associated with our oscillator alignment accuracy is about one-third of a mode diameter. Further alignment errors and alignment instabilities increase this offset. Major distortions of the pump beam appear to cause breakup of the oscillator mode, often leading to two lobe modes similar to a TEM_{01}. Finally, we have considered chromatic and off-axis aberrations in the telescopes, leading to spreading of the beam, as a possible cause of loss of Stokes signal. The change of focal length of lenses with wavelength typically changes a telescope which is afocal in the visible or red into effectively a negative lens in the near infrared. If f_1 and $-f_2$ are the nominal focal lengths of the two lenses making up the telescope, the resultant effective focal length for a dispersion $\Delta n = -\delta$ is given by

$$f_{eff} = -\left(\frac{n-1}{\delta}\right)\frac{f_1 f_2}{f_1 - f_2},$$

where n is the visible index of refraction. For a typical relative dispersion of $\delta/(n-1) = 0.01$ for the wavelength change of interest, our 10-power telescope becomes effectively a lens with -150 cm focal length. Off-axis effects would be most important at the negative lens of the 2.5-power telescope. Since this lens is only about twice the size of the beam and is located about 2 m from the 10-power telescope, the cumulative effect of offsets and alignment errors can be quite large.

Figure 9 shows some near field photographs of the Stokes oscillator output beam. The top row, Fig. 9(a) through (d), shows the beam with the 10-power telescope removed and the 2.5-power telescope in place, and indicates the progressive breaking up of the beam with added misalignment or pump beam distortion. The beam size is about 3mm. A reduced-size TEM_{00} mode should decay primarily through the TEM_{00}, TEM_{02}, and TEM_{20} modes of the passive cavity after the pump is removed; this feature can be seen in Fig. 9(a) through (c). The pattern in Fig. 9(d) occurred after the beamsplitter had been damaged. Since no aperture of the system is included in these photographs, offsets from the alignment axis cannot be deduced. The bottom row, Fig. 9(e) through (h), shows the beam with the 10-power telescope in place and the 2.5-power telescope removed. These photographs are overexposed to show the aperture of a beam-folding prism after the 10-power telescope, and therefore exaggerate the beam size and edge structure. The beam size is somewhat larger than 1 cm. Ideally, the beam should be centered in the prism aperture. Offsets, distortion, and breakup of the beam can be seen. The decaying Stokes radiation should overfill the prism aperture, and presumably provides the illumination of that aperture in these photographs.

With either the 10-power telescope or the 2.5-power telescope alone, the Stokes signal is not significantly attenuated. With both telescopes in the beam, about 13 dB attenuation is observed, and photographs of the beam show that the aperture of the telescope is grossly overfilled following the negative lens. Based on the above discussion, we conclude that offsets due to alignment errors, beam spreading due to focusing errors, errors in aligning a system of two telescopes separated by about 2 m with three beam-folding prisms between them, and the limited apertures of some components combine to move the beam off axis and spread and attenuate it to the degree we observe, even though no error is particularly damaging in itself.

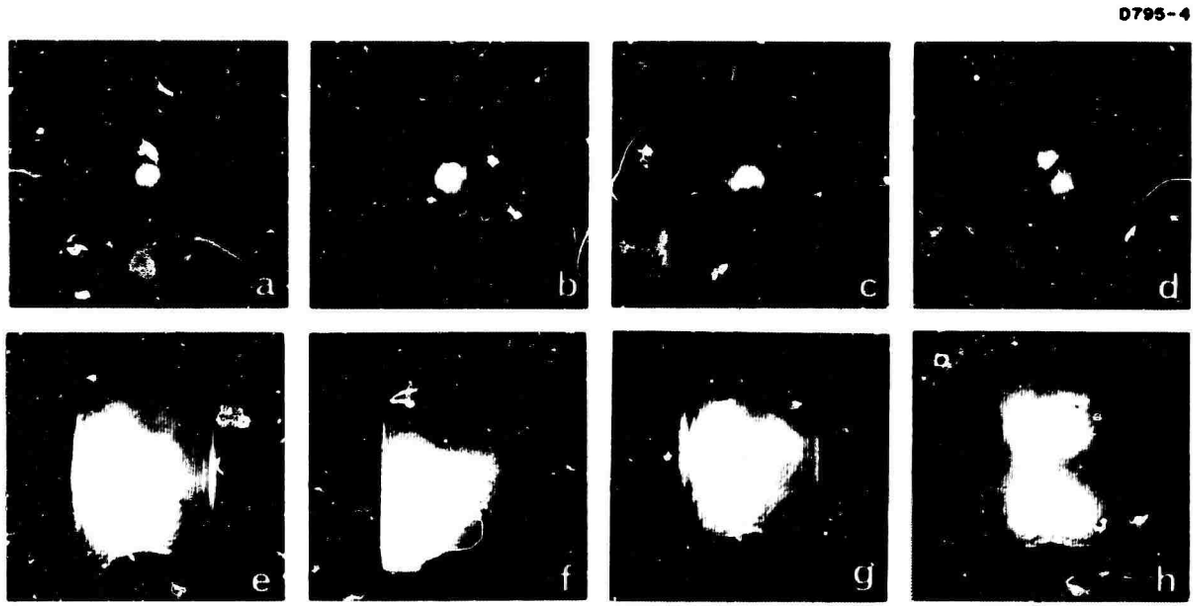

Fig. 9. Hydrogen Stokes oscillator near field photographs. Top row: after 2.5 power telescope, with 10-power telescope removed. Bottom row: after 10-power telescope, with 2.5 power telescope removed. See text.

4. Discussion

The H_2 Stokes oscillator-amplifier apparatus is rather complicated, in the sense that it has some components whose alignment is critical. This makes the system difficult to align and allows the development of cumulative errors.

Several modifications can be made to our system in order to alleviate the problems we encountered. These include the following:

a. Increase the mode size of the H_2 oscillator. This would considerably simplify coupling of the oscillator output into the amplifier. For a mirror spacing d/2 which is small compared with the radius R of the spherical mirror, the mode diameter

$$2\omega_o \approx 2\left(\frac{\lambda}{\pi}\right)^{1/2} (dR)^{1/4}$$

increases rather slowly with d and R. For large R, alignment and stability become problems. One solution would be to use a confocal or nearly confocal cavity. This would give the maximum spot size for a given radius mirror and very greatly reduce alignment and stability problems. In addition, the output could be taken from the spherical mirror, further increasing the output mode size. Another approach would be to use a small output mirror, leading to a small Fresnel number and relatively high diffraction loss. Such diffraction loss is quite effective in selecting the fundamental mode and the diffraction from the fundamental mode can provide the output beam.

b. Increase the transmission of the output mirror of the H_2 oscillator to match the cavity decay time to the pump pulse duration. This step would supply all of the energy stored in the cavity as useful power to be amplified by the pump pulse. The pump power to the oscillator of course would have to be increased to compensate for the added loss.

c. Decrease the distance between the two telescopes carrying the Stokes beam. This would simplify coupling of the H_2 oscillator output into the amplifier. In addition, the rearrangement would be made so that the entire system could be aligned without reversing the alignment telescope in its mount, eliminating that source of error.

d. Use a high field damage resistant dichroic mirror. In our apparatus this mirror is a flat with high reflectivity in the red. Such mirrors are available with high field damage resistant characteristics as a standard item.

e. Partially diffuse the H_2 oscillator pump beam. This would provide a more uniform and easily controllable pump. Using some of the above techniques of mode control, the pump beam need not be so constricted, and the effects of the rapid spatial variation of the gain would be circumvented.

The primary advantage of this design principle is that because a gaseous amplifying medium is used and the pump is not introduced from the side, the system can be scaled up to larger size. The only requirement is that the intensity be kept below the level where the amplifier becomes unstable. An amplifier chain thus could be constructed, separated by afocal telescopes to progressively increase the beam size and dichroic beamsplitters to introduce additional pump energy. The amplifier chain could include backward wave amplifiers in the final stages to yield very high power in a short pulse.

IV. THEORY OF THIRD ORDER POLARIZABILITY APPLIED TO HYDROGEN

A. Introduction

The major theoretical problem of the H_2 Raman laser which we have approached is that of understanding a rather complicated anomalous Raman output observed in parallel-beam-pumped H_2 gas cells with nonreflecting tilted, or Brewster angle, windows. The output is anomalous in the sense that it cannot be understood on the basis of the known Raman transition strength and measured cavity parameters. The anomalous behavior occurs at pressures above $\sim$ 10 atm, is insensitive to the higher pressures (up to $\sim$ 100 atm), and resembles that which would be expected if reflecting windows (of around 1% reflectivity) were present.[2, 3, 11, 13] We have considered dozens of possible sources of this behavior, from the effects of nonlinear absorption in impurities in the H_2 gas to stimulated normal and thermal Rayleigh wing scattering. Some of these possibilities have been discussed in previous reports. Upon further investigation, we have been able to discard most of such hypotheses. One rather complicated hypothesis, explained in Section V-F, must be investigated further. It presupposes the existence of a nonresonant nonlinearity, for which there is little evidence, and involves dielectric guiding effects stimulated by the pump beam at Raman shifted frequencies. Independent measurements of electronic nonlinearities in H_2 would be the most sensitive test that could be devised for this hypothesis at present. Such an effect need not affect H_2 Raman laser performance if beam diameters, pressures, and oscillator parameters are adjusted properly.

In the following sections we outline the derivation of the appropriate nonlinear susceptibility and the coupled wave theory appropriate to weak stimulated Raman scattering from a plane wave pump. All parameters are evaluated for H_2 according to the best present knowledge. The role of the nonresonant nonlinearities is established, and limitations imposed by transient effects are discussed. We begin this rather self-contained view of the theory with an important simplifying theorem on the form of the interaction Hamiltonian.

B. A Simplification in the Form of the Field-Molecule Interaction

From the most fundamental (nonrelativistic) viewpoint, the electromagnetic field couples to a charge in a molecule via a term in the Hamiltonian of the familiar form (in cgs units)

$$\frac{e}{2mc}\left[-\underset{\sim}{p}\cdot\underset{\sim}{A}(\underset{\sim}{x},t)-\underset{\sim}{A}(\underset{\sim}{x},t)\cdot\underset{\sim}{p}+eA^2(\underset{\sim}{x},t)/c\right]-e\phi(\underset{\sim}{x},t)$$

where e and m are the charge and mass of the particle, p is its momentum operator, and the $\underset{\sim}{A}(\underset{\sim}{x},t)$ and $\phi(\underset{\sim}{x},t)$ are the vector and scalar potentials of the electromagnetic field evaluated at the position $\underset{\sim}{x}$ of the particle. Calculation of the polarization to third order in $\underset{\sim}{A}$ and ϕ with this interaction leads to a rather complicated sum of delicately cancelling terms which are difficult to use for numerical calculations. We have been able to show that in the dipole approximation, this exact method of calculating the nonlinear polarization is equivalent to a much simpler one in which the above Hamiltonian is replaced by only one term $-\underset{\sim}{m}\cdot\underset{\sim}{E}(Rt)$ where $\underset{\sim}{m}$ is the dipole moment operator for the molecule and $\underset{\sim}{E}(\underset{\sim}{R}t)$ is the electric field at its center position $\underset{\sim}{R}$. This equivalence has not been evident to some workers. We shall employ the worthwhile simplification and numerical convenience of this latter form.

C. A Quantum Mechanical Expansion of the Nonlinear Polarization to Third Order in the Perturbing Electric Fields

We seek the expected value $M_i(t)$ of the i^{th} component of the electric dipole moment of an isolated molecule in an electric field whose components are $E_j(s)$. If the interaction Hamiltonian is $-m_i(t)E_i(t)$ in the unperturbed Heisenberg representation (repeated indices are assumed to be summed), a well-known quantum mechanical perturbation procedure gives

$$M_i(t) = i\int^t ds\,\langle m_i(t),\, m_j(s)\rangle E_j(s)$$

$$+ i^3\int^t ds\int^s du\int^u dv\,\langle[[[m_i(t), m_j(s)], m_k(u)], m_\ell(v)]\rangle$$

$$\cdot E_j(s)E_k(u)E_\ell(v) + \ldots\,, \qquad (1)$$

in which energies are measured in frequency units ($\hbar = 1$) and the brackets $\langle\rangle$ indicate the expected value for an unperturbed ($E_i = 0$) molecule. The lower time limits on the integrals are some time in the distant past before which the fields were absent and the molecule had the probability P_a of being in an energy eigenstate $|a\rangle$.

We shall assume that the electron field is a superposition of oscillating components $\Sigma_\beta E_{i\beta} \exp i\omega_\beta t$, of (plus and minus) frequencies ω_β, and complex amplitudes $E_{i\beta}$, where the amplitude of a minus frequency term is the complex conjugate of the corresponding positive frequency amplitude. (Greek subscripts refer to Fourier components.) We will then use (1) to find the amplitude $M_{i\nu}$ of the $\exp i\nu t$ component of polarization. Because we are considering only stimulated effects, ν is a linear superposition of any three of (±)the electric field frequencies. We write

$$M_{i\nu} = \alpha E_{i\nu} + \alpha_{ijk\ell}^{\beta\gamma\delta} E_{j\beta} E_{k\gamma} E_{\ell\delta} \tag{2}$$

where α is the usual linear polarizability and $\alpha_{ijk\ell}$ is the third order nonlinear polarizability for the case $\nu = \omega_\beta + \omega_\gamma + \omega_\delta$. We may now expand (1) in terms of matrix elements m_i^{ab} of the dipole moment m_i between states a and b(c, d, etc.) to obtain

$$\begin{aligned}
\alpha_{ijk\ell}^{\beta\gamma\delta} = \sum_{a,b,c,d} P_a \Bigg[& \frac{(ijk\ell,\ abcd)}{(\nu + \omega_{ba})(\nu_2 + \omega_{ca})(\omega_\delta + \omega_{da})} \\
& + \frac{(\ell kij,\ abcd)}{(\nu + \omega_{dc})(\nu_2 + \omega_{ac})(\omega_\delta + \omega_{ab})} \\
& - \frac{(jik\ell,\ abcd)}{(\nu + \omega_{cb})(\nu_2 + \omega_{ca})(\omega_\delta + \omega_{da})} \\
& - \frac{(\ell kji,\ abcd)}{(\nu + \omega_{ad})(\nu_2 + \omega_{ac})(\omega_\delta + \omega_{ab})} \\
& + \frac{(kji\ell,\ abcd)}{(\nu + \omega_{dc})(\nu_2 + \omega_{db})(\omega_\delta + \omega_{da})} \\
& + \frac{(\ell jik,\ abdc)}{(\nu + \omega_{dc})(\nu_2 + \omega_{db})(\omega_\delta + \omega_{ab})} \\
& - \frac{(kij\ell,\ abcd)}{(\nu + \omega_{cb})(\nu_2 + \omega_{db})(\omega_\delta + \omega_{da})} \\
& - \frac{(\ell ijk,\ abcd)}{(\nu + \omega_{cb})(\nu_2 + \omega_{db})(\omega_\delta + \omega_{ab})} \Bigg]
\end{aligned} \tag{3}$$

where the intermediate states b, c, and d are summed over all energy eigenstates, and the initial state a is summed with its statistical weight factor P_a. Here $\nu_2 = \omega_\delta + \omega_\gamma$, and the symbols (ijkℓ, abcd), etc., mean the products $m_i^{ab} m_j^{bc} m_k^{cd} m_\ell^{da}$, etc., of matrix elements. The frequency ω_{ab} is the energy of state $|a\rangle$ minus the energy of state $|b\rangle$, etc. Each factor in the denominators may be thought of as having a term $-i\Gamma_{ab}$, etc., representing the width of the particular transition in that factor.

In all the Raman H_2 amplifier and oscillator arrangements with which we are concerned, two of the three electric fields in the nonlinear factor of (2) are very nearly components of a linearly polarized plane wave pump field whose frequency components are at $\pm\nu_o$ with amplitudes $E_o \exp(-i\underset{\sim}{k}_o \cdot \underset{\sim}{R})$ and $E_o^* \exp(i\underset{\sim}{k}_o \cdot \underset{\sim}{R})$, respectively; $\underset{\sim}{k}_o$ is the (real) pump wave-vector and $\underset{\sim}{R}$ is the position of the molecule. Various processes, including coupled or pure Stokes and anti-Stokes Raman and Rayleigh scattering, and the dc and ac Kerr effects, are identifiable as arising from one or more of the terms in (3) with certain intermediate state combinations. We concentrate now on the coupled Stokes-anti-Stokes waves with which we must deal in the H_2 Raman maser.

D. Coupled Wave Equations for Stimulated Raman Scattering

We consider here the case of interest to the H_2 Raman maser where all wave polarizations are very nearly parallel, and therefore only one space component $\alpha_{xxxx}(\beta\gamma\delta)$ of the nonlinear polarizability tensor is involved. We will study only the case where the pump wave is essentially unattenuated by the scattering and the only important nonlinear terms in (2) are quadratic in the pump amplitude. That is, two of the three subscripts $\beta\gamma\delta$ refer to one of the two conjugate pump terms. The third subscript must refer either to a first Stokes or anti-Stokes wave in the Raman effect.

We must look for such terms in (3) which produce polarization at the first Stokes and anti-Stokes frequencies, assuming that the initial state a is the ground state of the Raman transition and that no dipole matrix elements exist except for electronic transitions (as is the case for H_2). The most important of such terms are resonant because the middle factor in a denominator nearly vanishes when the state c is the upper Raman level ($\nu_2 \approx \pm\omega_{ac}$); however, we will find that nonresonant contributions to α_{xxxx} may also be important to stimulated Raman characteristics.

The polarizability terms of the form (3) which are quadratic in pump amplitude will couple a Stokes polarization wave

$$P_s \exp - i(\underset{\sim}{k} \cdot \underset{\sim}{x} - \nu t) + c.c. \tag{4a}$$

to an anti-Stokes wave

$$P_a \exp - i[(2\underset{\sim}{k}_o - \underset{\sim}{k}^*) \cdot \underset{\sim}{x} - (2\nu_o - \nu^*)t] + c.c. \tag{4b}$$

These waves are accompanied by electric fields

$$E_s \exp - i(\underset{\sim}{k} \cdot \underset{\sim}{x} - \nu t) + c.c. \tag{4c}$$

and

$$E_a \exp - i[(2\underset{\sim}{k}_o - k^*) \cdot \underset{\sim}{x} - (2\nu_o - \nu^*)t] + c.c. \tag{4d}$$

Equating the terms in Maxwell's equations that have the same space and time dependence gives

$$P_s = \left(X_{ss} + X_s^o\right)E_s + X_{sa}\, E_a^* \tag{5a}$$

$$P_a^* = X_{as}\, E_s + \left(X_{aa} + X_a^o\right)E_a^* \tag{5b}$$

where X_ε^o and X_a^o are the normal linear susceptibilities and the nonlinear susceptibilities X_{sa}, etc., are equal to $\rho a_{sa} L_{sa}$. Here ρ is the number density, L_{sa} are local field correction factors approximately related to the Stokes (anti-Stokes) indices of action, $n_s(n_a)$, by $L_{sa} = (n_s^2 + 1)^2 (n_a^2 + 1)^2/81$, etc., and the polarizabilities a_{sa} are obtained from (3). The resonant parts of these polarizabilities are seen to be (for the case of parallel polarizations and a molecule certainly in the lower Raman level a)

$$\chi_{ss} = |E_o|^2 \sum_{b,d} \frac{(xxxx, abcd)}{D} \left(\frac{1}{\omega_{ba} + \nu} + \frac{1}{\omega_{bc} - \nu}\right)$$

$$\cdot \left(\frac{1}{\nu + \omega_{da}} + \frac{1}{\omega_{da} - \nu_o}\right) \tag{6a}$$

$$\alpha_{sa} = E_o^2 \sum_{b,d} \frac{(xxxx, abcd)}{D} \left(\frac{1}{\nu + \omega_{ba}} + \frac{1}{\omega_{bc} - \nu} \right)$$

$$\cdot \left(\frac{1}{\omega_{da} - 2\nu_o + \nu^*} + \frac{1}{\omega_{da} + \nu_o} \right) \qquad (6b)$$

$$\alpha_{aa} = |E_o|^2 \sum_{b,d} \frac{(xxxx, abcd)}{D} \left(\frac{1}{\omega_{ba} - 2\nu_o + \nu^*} + \frac{1}{\omega_{bc} + 2\nu_o - \nu^*} \right)$$

$$\cdot \left(\frac{1}{\omega_{da} - 2\nu_o + \nu^*} + \frac{1}{\omega_{da} + \nu_o} \right) \qquad (6c)$$

$$\alpha_{as} = E_o^{*2} \sum_{b,d} \frac{(xxxx, abcd)}{D} \left(\frac{1}{\omega_{ba} - 2\nu_o + \nu^*} + \frac{1}{\omega_{bc} + 2\nu_o - \nu^*} \right)$$

$$\cdot \left(\frac{1}{\omega_{da} + \nu} + \frac{1}{\omega_{da} - \nu_o} \right) \qquad (6d)$$

where D is the resonant denominator $\omega_{ca} + \nu - \nu_o + i\Gamma_{ca}$. It has often been assumed that $\alpha_{ss} = \alpha_{sa} = \alpha_{as} = \alpha_{aa}$. This is seen to be the case in the limit where all the wave frequencies are much lower than the energy differences ω_{ba}, ω_{bc}, ω_{da}. This would also result with the Plazcek model of coupling via a polarizability change that is proportional to the amplitude of the Raman vibration. However, with most materials even more than with H_2, this limit is not reached. In order to estimate the differences of these coefficients for the Q_{01} (1) Raman transition of H_2 we assume that the intermediate state sums in (6) are imitated by pretending that there is only one intermediate level b whose energy difference from the initial state, ω_{ba}, is 90,000 cm^{-1} (a value which, if used to calculate the linear polarizability, gives a good fit for optical dispersion). The Q_{01} (0) frequency ω_{ca} is 4155.2 cm^{-1} and the ruby pump frequency ν_o is 14,402 cm^{-1}. With these values we find

$$\alpha_{ss}:\alpha_{sa}:\alpha_{aa}:\alpha_{as} = 1:1.01:0.83:0.95 , \qquad (7)$$

which will appreciably alter predictions of relative anti-Stokes intensities and the gain near the index-matched emission angles for H_2 at pressures around 10 atm or more. Our own numerical analyses, however, indicate that this effect does not predict any gain anomalies such as those that we and others have observed.

The nonresonant corrections to (6) from (3) are of many physical origins. We have studied the various types of nonresonant terms and found that the "electronic" contributions, where b, c, d are all excited electronic states, probably dominate the "nuclear" terms, in which c is a component state of the ground electronic level. Terms at ν of the latter type arise from the tails of neighboring Raman transitions (especially from Q_{01} (0)), and Kerr and Rayleigh type effects.

As a result of two investigations, we believe that the electronic contributions to the X_{sa} are important to any quantitative understanding of stimulated Raman effects. First, knowing the locations of the important lower lying singlet electronic levels of H_2 from published spectroscopic data, we have estimated that some energy denominators of (3) can be quite small, nearly resonant, for the wave frequencies of interest. Hence, the sum over all intermediate electronic states need not be small compared with the resonant Raman terms exhibited in (6). Second, in the Landolt-Bornstein tables a value exists for the dc Kerr constant of liquid H_2 (19^oK) taken from some unpublished measurements, equal to 4×10^{-9} esu. We have worked out the quantum theory of this Kerr constant, assuming that it arises entirely from molecular reorientation, and found a predicted value several orders of magnitude lower than this reported value. This means that either the reported value is in error, or that it arises from purely electronic nonlinearities. If we assume the latter and suppose that the pump field E_o is equally as effective in producing a polarizability change at the Stokes frequency $\delta\alpha_{ss}$ as the dc field in the Kerr measurement (this could be false because of changing energy denominators), the $\delta\alpha_{ss}$ is of the order of the maximum of $Re\alpha_{ss}$ of (6) at 10^3 atm pressure. We will need to assume for our purposes that this occurs rather at 10 atm.

The effects of these nonresonant terms in the X_{ij} are difficult to guess in the absence of any knowledge of their relative signs or sizes. They are not generally equivalent to index changes at the two frequencies because the cross terms X_{sa}, X_{as} produced gain and quite different effects from index changes. However, when the on-axis Stokes waves are far from being index-matched, as they are at the pressures (20 to 100 atm) at which our H_2 Raman lasers are commonly operated, it appears likely that the main effect will be to produce a simple index

change δn_ν which is proportional to the pump intensity. Qualitative agreement with experiments would result if we assumed this change to be at a pressure P_{atm} (atmospheres) and pump $I_o MW/cm^2$,

$$\delta n_\nu \cong 2 \times 10^{-9} P_{atm} I_o . \qquad (8)$$

In order to obtain an idea of the tendency of such an index change to self-focus, note that under the typical operating conditions, $P_{atm} = 100$ and $I_o = 20$, this change in index would cause total internal reflection of a beam at 3 mrad to a plane at which the change occurred suddenly. The effects of these nonresonant terms on beam coherence may well be comparable with the focusing effects arising from the gain variation across the pump beam. These latter effects have been discussed by Kogelnik and Yariv and were considered earlier in this report in connection with the observation of mode pinching and pinning.

E. Maxwell's Equations for Coupled Waves

The nearly collinear field and polarization, Stokes-anti-Stokes waves (4) obeying the relations (5) are solutions of Maxwell's equations if

$$[-k^2c^2 + \nu^2(n_s^2 + 4\pi X_{ss})] E_s + 4\pi \nu^2 X_{sa} E_a^* = F_s \qquad (9a)$$

$$[-k_a^2c^2 + \nu_a^2(n_a^2 + 4\pi X_{aa})] E_a^* + 4\pi \nu_a^2 X_{as} E_s = F_a \qquad (9b)$$

where $k_a = 2k_o - k^*$ and $\nu_a = 2\nu_o - \nu^*$. The driving forces F_s and F_a include external signals and noise terms which are correctly given by applying the quantum Nyquist's theorem for parametric amplifiers. We will be interested mainly in the gains and oscillator thresholds, so that it will be sufficient to study the homogeneous form of (9) (i.e., to solve the determinant of the coefficients of the LHS of (9) for possible values of k and ν). Results of this are summarized below.

F. Steady State

The steady state solutions for the infinite plane wave pump are obtained by finding the complex $\underset{\sim}{k} = \underset{\sim}{k}' + i\underset{\sim}{k}''$ which satisfies (9) for a

given real positive ν. Those solutions for $\underset{\sim}{k}$ which have the largest imaginary parts k'', and hence the most gain, will be most effective in amplifying external signals and will have the lowest thresholds for oscillation for a given amount of feedback. Fixing the directions of $\underset{\sim}{k}'$ and $\underset{\sim}{k}''$ as well as ν and putting the complex determinant for (9) equal to zero gives the magnitudes k' and k'' of $\underset{\sim}{k}'$ and $\underset{\sim}{k}''$. Since the results are insensitive to the direction of $\underset{\sim}{k}''$, provided that $k'' \ll k'$ and $\underset{\sim}{k}''$ is directed near the forward direction as we have supposed, we shall take $\underset{\sim}{k}''$ to be parallel to the unit vector $\underset{\sim}{u}$ in the direction of $\underset{\sim}{k}'$. That is, we will look for solutions of the form

$$\underset{\sim}{k} = \underset{\sim}{u}k = \underset{\sim}{u}(k' + ik'') . \tag{10}$$

If we define the dimensionless deviation of k from its normal value by

$$G = [kc/(n_s \nu)] - 1 \tag{11}$$

and define the dimensionless nonlinear susceptibility parameters

$$Z_{sa}(\nu) = 2\pi X_{sa}(\nu)/(n_s n_a) \tag{12}$$

and so forth for Z_{ss}, etc., and also define an index mismatch parameter for the small angle θ between $\underset{\sim}{k}_o$ and $\underset{\sim}{k}$ by

$$V = \frac{1}{2}[\nu_a^2 n_a^2 - (2\nu_o n_o - \nu n_s)^2 - 2\theta^2 n_o \nu_o n_s \nu]/(n_a \nu_a)^2 , \tag{13}$$

then the determinant of the coefficients of (9) gives the quadratic equation for G

$$(G - Z_{ss})(AG + V + Z_{aa}) + Z_{sa} Z_{as} = 0 \tag{14}$$

where we have neglected terms of order k''/k', θ^2, and G (which is of order Z) smaller. The parameter $A \equiv (2\nu_o \nu n_o n_s - n_s^2 \nu^2)/(n_a \nu_a)^2$

is nearly ν_s/ν_a for H_2 gas. Recall that the linear indices of refraction at the frequencies ν, ν_o, and ν_a are n_s, n_o, and n_a. The so-called normal Stokes index-matched emission angle θ_o is obtained by putting $V = 0$. The normal unmatched Stokes (or anti-Stokes) gain is seen to be $G = Z_{ss}$ (or $\Delta G = -\nu - Z_{aa}$).

For the H_2 Q_{01} (1) Raman transition

$$V(\theta) = 8.89 \times 10^{-7} P_{atm} - 0.429\, \theta^2, \qquad (15)$$

yielding a matched Stokes angle $\theta_o = 1.43\, P_{atm}^{1/2}$ mr, and

$$A = 0.553\,. \qquad (16)$$

It is convenient to write

$$Z_{ss} \approx [\beta I_o c/(2n_s\nu)]\, i\Gamma/(w - \nu_o + \nu - i\Gamma) + z_{ss}] \qquad (17)$$

where β is the "peak gain constant" for uncoupled Stokes waves and is generally taken to be 1.5×10^{-3} cm/MW for the pressure broadened Q_{01} (1) line of halfwidth 2Γ and Raman shift $w/(2\pi c) = 4155.2$ cm^{-1}. The nonresonant component of Z_{ss} is represented by z_{ss}, which, if (8) were correct, is

$$z_{ss} \approx 0.2\, P_{atm}\,. \qquad (18)$$

Although at present the relations of the Z_{sa}, z_{sa}, etc., to Z_{ss} are not well known, an idea of the quality of the actual gain solutions can be obtained by assuming $Z_{aa} = Z_{ss} = Z_{sa} = Z_{as} \equiv Z = Z' + iZ''$, as would follow from the Plazcek model plus equal nonresonant terms. The determinantal equation (14) then gives for the solutions $G_\pm$:

$$2AG_\pm = -V - Z(1 - A) \pm \{[V + Z(1 + A)]^2 - 4A\, Z^2\}^{1/2} \qquad (19)$$

When $z_{ss} < 0.1$ the maximum gain occurs when V is as large as possible, that is, at angles as far from index matching as possible. However, when $z_{ss} \gtrsim 1$, the maximum gain occurs near the angle θ_m where $V = -Z'(1 + A)$, if that is possible, i.e., for

$$\theta_m \approx [2.07 \times 10^{-6} P_{atm} + 1.04 Z']^{1/2} . \qquad (20)$$

For the case of a large nonresonant susceptibility ($z_{ss} \gtrsim 1$), the largest G'' evidently occurs near a frequency where Z' is most positive (i.e., for $w - \nu_o + \nu \sim -\Gamma$ where ν is on the low frequency side of the Stokes line peak). The nonresonant term z_{ss} is positive and, above several atmospheres pressure, would contribute the major portion of Z' if (18) is a good approximation. This nonresonant portion Z^{NR} would be $\sim 1.17\ 10^{-8}\ z_{ss} I_o \sim 2.3 \times 10^{-9} I_o P_{atm}$ and therefore $\theta_m \sim \theta_o$ for $I_o < 10^3$ MW/cm^2. For our operating pressures and if (18) is correct, we see from (19) that the root G with the most gain is nearly

$$G_+ = i\ 1.345Z' - i\ 0.405Z'' , \qquad (21)$$

which is greater than the normal peak Stokes gain $-iZ_{ss}(\nu_o - w) = G_o$ if $z_{ss} \gtrsim 1$. For very large $z_{ss} \gg 1$, ($P_{atm} \gg 5$), the largest G_+'' is at the frequency given by $(\nu_o - \nu - w)/\Gamma \approx 1.34$ and is

$$G_+''/G_o \rightarrow 1.345\ z_{ss} + 0.372. \qquad (22)$$

We have seen after (20) that at the moderate I_o (< 500 MW/cm^2) at which our lasers operate, the angle of optimum gain θ_m is only slightly below the index matched angle θ_o, which for a typical operating pressure of 50 atm is 10 mrad. Furthermore, the gain falls off very rapidly away from this angle. If the pump beam divergence were much less than θ_o, one might suppose that the Raman wave could not take advantage of optimum gain for more than a certain length before the coupled waves would diverge from each other in space. This would not be true, however, if the nonlinear index (ReG) of the coupled Stokes-anti-Stokes pair were large enough to confine the wave within the bounds of the pump beam by a dielectric waveguide effect. This confinement would occur rather suddenly as the pump power increased and would bring on a sudden increase in the single pass gain. It is in such a way

that we propose that the sudden onset of large stimulated Raman outputs (as pump power is increased) may be understood. A more quantitative understanding obviously would have to come from a study of waves of finite cross-sectional area rather than of the coupled infinite plane waves we have been considering. However, even without the complete theory, one can obtain a qualitative picture. The increase in index δn required to totally reflect a wave at a plane by a small angle θ_m is $\theta_m^2/2$. If (8) is roughly correct, this means that, for $2 \times 10^{-9} m$ $I_o P_{atm} \sim (1.4)^2 P_{atm} \times 10^{-6}/2$ (that is, at $I_o \sim 5 \times 10^2$ MW/cm^2), a threshold for dielectric guiding of the high gain waves should appear. This crude estimate is near enough to the observed thresholds of $\sim$ 40 MW/cm^2 to make promising a further investigation of the hypothesis. One might say that since in the H_2 oscillators and amplifiers the complications of this extra "parametric" gain and dispersion are unwanted, perhaps one should work at low pressures, $\sim$ 5 atm, where the Raman gain is not much reduced but the parametric effects would be. Unfortunately, transient effects appear to become important at pressures below several tens of atmospheres, for the reasons we discuss in the next section. Therefore, nonresonant parametric effects may well appear in a practical system.

G. Transient Behavior

To analyze the transient buildup of a wave packet after a plane wave pump of constant amplitude has been turned on, we write the initial wave packet as a superposition of plane waves of the form (4) with different real $\underset{\sim}{k}$. Maxwell's equations (9) are then satisfied by a complex $\nu(\underset{\sim}{k}) = \nu'(\underset{\sim}{k}) + i\nu''(\underset{\sim}{k})$ for each $\underset{\sim}{k}$. The wave packet at a time t later is given by superposing the original $\underset{\sim}{k}$ components with each modified by a factor $\exp i\nu(\underset{\sim}{k})t$. As usual, a smooth wave packet whose spatial extent is longer than [the linewidth cm^{-1}]$^{-1}$ usually travels with slowly changing shape with a group velocity whose vector components are $\delta\nu'/\delta k_i$. The packet grows in amplitude as $\exp(-\nu'')t$, a negative $\nu''(k)$ indicating gain.

To find ν it is useful to express it in terms of the dimensionless parameter U:

$$\nu = (kc/n_s)(1 + U), \tag{23}$$

from which Maxwell's equations (9) for the couple waves give

$$(U + Z_{ss})(AU - V(\theta) - Z_{aa}) + Z_{sa} Z_{as} = 0 \tag{24}$$

where A and V are as given after (14) but evaluated at $\nu = ck/n_s^2$, $\nu_o = ck_o/n_o^2$, and $\nu_a = ck_a/n_a^2$ so that their values are still as given in (15) and (16) for H_2 gas nea Raman shifts and at not too high pressures (so that $n_s - 1 \ll 1$). From (17) we see that we may now write

$$Z_{ss} = G_o[\ (UQ + B - i)^{-1} + z_{ss}] \tag{25}$$

where

$$B \equiv (w - \nu_o + ck/n_s)/\Gamma \tag{26}$$

is a dimensionless measure of the distance off resonance of the k being considered and

$$Q \equiv ck/(n_s\Gamma) \tag{27}$$

is one-half what would usually be called the "Q" of the Raman transition. In the pressure broadened region ($P_{atm} > 5$),

$$Q \approx 10^7/P_{atm} \tag{28}$$

for the Q_{01} (1) transition at 300°K.

It is evident from (25) that U generally satisfies a complex quartic equation. The four roots correspond to the normal Stokes and anti-Stokes electromagnetic waves and two "vibrational" waves in the matter when coupling is turned off. In the special case of the classical Plazcek picture for the matter vibration, there is an obvious cancellation and (24) reduces to a cubic equation in U, since there is only one possible matter wave in this picture. In any case we are interested in the solution U which has the most negative imaginary part U".

We will limit our considerations here to the case where $V(\theta=0)$ is so large that the nearly pure Stokes root given by $U + Z_{ss} = 0$ has most gain. This is the case of interest when the index matched angle

(where V = 0) is large enough and the nonlinear index effects are small enough that we have an ideal Stokes amplifier or oscillator employing axial waves of very small transverse wave-vector content. We will then see how wave packet growth rates saturate, an effect which sets a certain minimum P_{atm} at which efficient operation is possible. To study this Stokes root we will not write the z_{ss} term explicitly, but will simply modify the index of refraction to include it ($n_s^2 + G_o z_{ss} \rightarrow n_s^2$) because in this case it has only the effect of a negligible simple index change. The Stokes root U_s is then, from (24) and (25),

$$2QU_s = (i - B)\{[1 + 4QG_o/(i - B)^2]^{1/2} - 1\} \qquad (29)$$

which at small gains ($4QG_o \ll 1$) gives

$$U_s \approx G_o/(i - B), \qquad (30)$$

which varies with ck/n_s just as does the normal Raman resonance and peaks at B = 0 where the time gain per radian is G_o just as was the spatial gain per radian. We may break up the solution (29) into expressions for the real and imaginary parts U_s' and U_s''. For small B (i.e., near line center) these become

$$-QU_{so}'' = \frac{1}{2}(\sqrt{1 + 4QG_o} - 1) \qquad (31)$$

$$U_{so}' = -BU_{so}''/\sqrt{1 + 4QG_o}\ . \qquad (32)$$

Thus we see that when $QG_o \geq 1$, the peak gain U_{so}'' continues to rise, but more slowly, as $\sqrt{G_o/Q}$ rather than as G_o. A plot of this result was given in Fig. 3, Section II, showing how the time gain constant saturates with increasing pump powers. $G_oQ \sim 1$ means that the normal steady state gain per centimeter is of the order of the Raman linewidth (in cm^{-1}). The group velocity for an axial wave packet v_g is

$$v_g = (c/n_s)(1 + U' + QdU'/dB), \qquad (33)$$

and from (32) this becomes

$$n_s v_g/c = 1 - \frac{1}{2}[1 - (1 + 4G_o Q)^{-1/2}], \qquad (34)$$

showing that the group velocity drops to half its normal value in the limit of high gain.

The apparent saturation of gain for a wavepacket arises when the buildup and decay of field at a molecule is fast enough that its Fourier components lie outside the amplifying bandwidth (2Γ rps) of the molecule. It was found experimentally that P_{atm} had to be greater than 20 atm if no gain saturation was to be evident.

BLANK PAGE

V. SUMMARY

Liquids were found to be much more limited than H_2 gas in potential performance in Raman lasers because of nonlinear index effects. Symmetric-molecule liquids are the best in this regard. In these, the origin of the nonlinear index in all cases of interest was found to be molecular redistribution, dominating electronic nonlinearities by at least an order of magnitude. We were able to show theoretically (Appendix I) that simple dc Kerr measurements will give the optical nonlinear index very closely if one assumes that the difference in indices measured in the Kerr effect is 3/2 the optical nonlinear index change. Available Kerr measurements show that the very best liquids for Raman lasers cannot handle more than several megawatts without the formation of beam instabilities.

The prototype H_2 gas Raman oscillator-amplifier we have constructed and tested demonstrated brightness gains of 20 dB and absolute brightness output of $\sim 10^{14}$ W-cm^{-2} sr^{-1} by the end of the contract period. The potential output of 10^{16} W-cm^{-2} sr^{-1} was not yet obtained with the 5 J ruby laser pump pulse available, probably as a result of noncritical technical difficulties. A possible theoretical model which we have proposed of the anomalous behavior of the H_2 Raman amplifier observed under certain operating conditions could be checked with standard nonlinear index measuring techniques. We have found no fundamental difficulties that would prevent extension of the technique to achieve brightnesses $\sim 10^{17}$ W-cm^{-2} sr^{-1} or higher. We feel that our work shows that this Raman technique would produce brightnesses up to 10^{17} for fewer dollars per W-cm^{-2} sr^{-1} than any other means presently available. Table V summarizes the brightness values presently obtained and those which could possibly be obtained with our existing laser systems.

TABLE V

Laser Brightness

System	Present Performance, $W\text{-}cm^{-2}\ sr^{-1} \times 10^{15}$	Possible Performance and Conditions, $W\text{-}cm^{-2}\ sr^{-1} \times 10^{15}$
Ruby Giant Pulse Oscillator	0.4	2.0 Shorter pulse and more complete transverse mode control
Ruby Giant Pulse Oscillator and Amplifier	0.025	2.5 Best current technology for crystals and laser design
H_2 Oscillator	0.08	0.4 Improved output coupling and pump techniques
H_2 Oscillator plus H_2 Amplifier	0.1	30 Near diffraction limited, strongly saturated output from our device

REFERENCES

1. R. W. Hellwarth, Phys. Rev. 152, 156 (1966).

2. P. V. Avizonis, A. H. Guenther, T. A. Wiggins, R. V. Wick, and D. H. Rank, Appl. Phys. Letters 9, 309 (1966).

3. P. V. Avizonis, K. C. Jungling, A. H. Guenther, R. M. Heimlich, and A. J. Glass, J. Appl. Phys. 39, 1752 (1968).

4. D. H. Close, C. R. Giuliano, R. W. Hellwarth, L. D. Hess, F. J. McClung, and W. G. Wagner, IEEE J. Quantum Electron. QE-2, 553 (1966).

5. R. W. Hellwarth, F. J. McClung, W. G. Wagner, and D. Weiner, J. Appl. Math. Phys. 16, 27 (1965).

6. E. Garmire, Physics of Quantum Electronics, P. L. Kelley, B. Lax, and P. E. Tannenwald, Eds. (McGraw-Hill, New York, 1966), p. 167.

7. N. Bloembergen and P. Lallemand, Phys. Rev. Letters 16, 81 (1966).

8. C. C. Wang, Phys. Rev. Letters 16, 344 (1966).

9. D. Weiner, S. E. Schwarz, and F. J. McClung, J. Appl. Phys. 36, 2395 (1965).

10. R. Hellwarth, N. George, and C. Cooke (to be published).

11. N. Bloembergen, G. Bret, P. Lallemand, A. Pine, and P. Simova, IEEE J. Quantum Electron. QE-3, 197 (1967).

12. G. G. Bret and M. M. Denariez, Phys. Letters 22, 583 (1966).

13. G. Bisson, G. Bret, M. Denariez, F. Gires, G. Mayer, and M. Paillette, Chim. Phys. 1, 197 (1967).

14. G. D. Boyd and H. Kogelnik, Bell System Tech. J. 41, 1347 (1962).

15. H. Kogelnik, Appl. Optics 4, 1562 (1965).

16. L. Casperson and A. Yariv, Appl. Phys. Letters 12, 355 (1968).

17. A. Yariv, Post-deadline paper presented at the Fifth International Quantum Electronics Conference, Miami, Florida, 14-17 June, 1968.

BLANK PAGE

DOCUMENT CONTROL DATA - R&D

(Security classification of title, body of abstract and indexing annotation must be entered when the overall report is classified)

1. ORIGINATING ACTIVITY *(Corporate author)*
Hughes Research Laboratories
3011 Malibu Canyon Road
Malibu, California 90265

2a. REPORT SECURITY CLASSIFICATION
Unclassified

2b. GROUP
N/A

3. REPORT TITLE
STUDY OF FUNDAMENTAL REQUIREMENTS FOR HIGH BRIGHTNESS RAMAN LASER SOURCES

4. DESCRIPTIVE NOTES *(Type of report and inclusive dates)*
Final Report; 1 October 1966 through 30 June 1968

5. AUTHOR(S) *(First name, middle initial, last name)*
McClung, F. J., Close, D. H., and Hellwarth, R. W.

6. REPORT DATE	7a. TOTAL NO. OF PAGES	7b. NO. OF REFS
July 1968	82	17

8a. CONTRACT OR GRANT NO.	9a. ORIGINATOR'S REPORT NUMBER(S)
NO 0014-67-C-0206	N/A
b. PROJECT, TASK, WORK UNIT NOS.	
ARPA Order No. 306	
c. DOD ELEMENT	9b. OTHER REPORT NO(S) *(Any other numbers that may be assigned this report)*
d. DOD SUBELEMENT	N/A

10. DISTRIBUTION STATEMENT

Qualified requesters may obtain copies of this report from DDC.

11. SUPPLEMENTARY NOTES	12. SPONSORING MILITARY ACTIVITY
	Physical Sciences Division Office of Naval Research Washington, D. C. 20360

13. ABSTRACT

We have studied stimulated Raman scattering (SRS) and nonlinear index effects in liquids composed of spherically symmetric molecules. We conclude that although SRS can be observed without self-focusing, nonlinear index effects, presumably because of molecular redistribution, are present and should lead to beam instabilities at somewhat higher powers.

We also have studied SRS in hydrogen gas pumped by a giant pulse ruby laser. We determined the stability conditions for various cell configurations and lengths. We designed and tested an H_2 Stokes oscillator which reliably produced up to 200 kW of Stokes power in a nearly diffraction-limited fundamental mode. An H_2 Stokes amplifier with over 30 dB small signal gain was built. While tests indicated that an amplifier output brightness of over 10^{16} W-cm^{-2} sr^{-1} could be obtained with the input provided by the H_2 Stokes oscillator, only 10^{14} W-cm^{-2}sr^{-1} was achieved because of difficulties in coupling the oscillator output into the amplifier. These difficulties resulted from the particular configuration used rather than any fundamental limitation.

Finally, we have made a theoretical study of the third order polarizability applied to hydrogen, and the resulting coupled Stokes-anti-Stokes waves. The study included steady state and transient behavior, as well as some possible explanations for the anomalous Stokes output from hydrogen gas.

DD FORM 1 NOV 65 1473

14. KEY WORDS	LINK A		LINK B		LINK C	
	ROLE	WT	ROLE	WT	ROLE	WT
Laser						
Raman scattering						
Nonlinear optics						
Liquids						
Gases						
H_2						
Self Focusing						
High Brightness						

APPENDIX I

EFFECT OF MOLECULAR REDISTRIBUTION ON THE NONLINEAR REFRACTIVE INDEX OF LIQUIDS

(Reprinted from The Physical Reveiw, Vol. 163, 205-206, 1967)

Reprinted from THE PHYSICAL REVIEW, Vol. 163, No. 1, 205-206, 5 November 1967
Printed in U. S. A.

Effect of Molecular Redistribution on the Nonlinear Refractive Index of Liquids. R. W. HELLWARTH [Phys. Rev. 152, 156 (1966)]. We have discovered an important error in the sign of a term calculated in the Appendix. As a result, the question raised in this paper as to the accuracy of the Kirkwood superposition approximation for calculating certain configurational averages for liquids can now be answered: The approximation gives the wrong sign at liquid densities for the nonlinear free-energy term and also for other quantities whose signs are known on general grounds. Specifically, in Eq. (A17), for I_3 the factor $(\beta+2\pi^2/3)$ should be $(\beta-2\pi^2/3)$. Also, in (A21) the factor 0.5066 should be replaced by 0.922 and in (A22) the factor -0.117 should be replaced by -0.467. We have re-examined the small correction K_4 and ascertained that its sign is negative, so that it contributes, though very little, to the worsening of the failure of the superposition approximation. With these corrections, the superposition approximation gives, instead of the existing Eq. (38),

$$U_{22}/(NE'^4\rho^3\alpha^4) = (\beta+2\pi^2/3)\Delta-2\pi^2/3 + \pi^2(32+136\Delta+167\Delta^2)/(45\rho\tau) + 1.13\rho\tau(1+K_4/4). \quad (38)$$

From the definition (28b), U_{22} must be positive. For symmetric molecules ($\Delta=0$), the right-hand side is seen to fail to stay positive as the density ρ increases beyond $1.6/\tau$, where $\tau/8$ is the molecular volume. Normal liquid densities run between $2/\tau$ and $3/\tau$. The above change in U_{22} requires that the expression (41) for n_2 be altered to

$$n_2=\frac{\pi\rho\alpha^2\beta}{n(1-4\pi\rho\alpha/3)^4}\left[\Delta+\frac{4\pi^2\rho\alpha^2}{45\tau}(32+136\Delta+167\Delta^2) + \frac{8\pi^2\rho^2\alpha^2(\Delta+1)}{3}+4.51\alpha^2\rho^2\tau\right], \quad (41)$$

which should also always be positive. The first two columns of Table I, which were calculated with the wrong Eq. (41), have no significance, except to indicate roughly the relative magnitude of the factor $\rho\alpha^2\beta n^{-1}(1-4\pi\rho\alpha/3)^{-4}$, which will exist even when a more accurate method than the superposition approximation is found.

We have looked for other obvious failures of the Kirkwood approximation and have found several. Kirkwood [J. Chem. Phys. 4, 592 (1963)] calculated corrections to the Clausius-Mossotti formula which, in the limit of small polarizability α, would be exact for all densities if one used exact correlation functions instead of the superposition approximation. These corrections change from positive to negative as the density increases beyond around $2/\tau$. This contradicts the demonstration in the present paper that the Clausius-Mossotti formula is a lower bound for the dielectric constant. Another typical failure of the superposition approximation occurs in the calculation of the positive quantity $\langle\Sigma_{\alpha\beta\gamma}D_{\alpha\alpha}{}^{\alpha\beta}D_{\alpha\alpha}{}^{\beta\gamma}\rangle/N-\langle\Sigma_{\alpha\beta}D_{\alpha\alpha}{}^{\alpha\beta}/N\rangle^2$ for which it gives [with Eq. (37)] $64\pi^2\rho^2/(45\rho\tau)-2\pi^2\rho^2/3$, a negative result when $\rho>32/15\tau$. The failure cannot be traced to the fact that with Eq. (A1), $\int p_4 d\mathbf{r}_4/V$ deviates slightly from p_3, etc.

The following typographical errors should be noted. A minus sign should be inserted before one side of (3). In the exponent of the right-hand side of Eq. (24), "$\mu_2-\mu_1$" should read "u_2-u_1". In the second line of the first paragraph, second column, of p. 161, "$\frac{1}{2}\tau$" should read "$\frac{1}{8}\tau$". The term $4\langle\langle u_2\rangle\rangle^2$ in Eq. (A19) and the left-hand side of Eq. (A23) should be divided by $\alpha^4E'^4$.

The conclusion is reached that there is no consistent usable approximation scheme for computing the configuration averages required to estimate the contribution of molecular redistribution to the nonlinear index n_2 of liquids. However, Eq. (41), which comes from the Kirkwood superposition approximation, should be accurate for molecular densities below those at which the inconsistencies discussed above appear.

APPENDIX II

KERR EFFECT IN SYMMETRIC-MOLECULE LIQUIDS

(Reprinted from Research Report No. 378)

HUGHES RESEARCH LABORATORIES
Malibu, California

a division of hughes aircraft company

Research Report No. 378

KERR EFFECT IN SYMMETRIC-MOLECULE LIQUIDS*

R. W. Hellwarth
Theoretical Studies Department

December 1967

*This paper is to be published in the Proceedings of the International School of Physics "Enrico Fermi" – XLII Course.

The work has been supported in part as a part of Project DEFENDER under the joint sponsorship of the Advanced Research Projects Agency, the Office of Naval Research, and the Department of Defense.

TABLE OF CONTENTS

I. INTRODUCTION

Around 1875, Kerr discovered that when a liquid is immersed in a uniform electric field, its optical index of refraction for light polarized parallel to this field changes by an amount $\delta n_{//}$, that is different from the change $\delta n_{\perp}$ for light polarized perpendicular to the field.[1] The effect exists either if the strong applied field is constant in time (DC Kerr effect) or if it oscillates at a frequency too high to be followed by any nuclear motions (AC Kerr effect). In the first case reorientation of permanent dipole moments may contribute to the effect, but not in the second case. We shall refer in what follows only to cases where a permanent dipole moment either does not exist or plays no role. Then the Kerr effect is generally explained as arising from the tendency of asymmetric molecules to lower their interaction energy with the strong field by reorienting themselves so that their axes of maximum polarizability tend to be along the field.[1,2] However, the Kerr effect in liquids of nominally symmetric molecules is comparable to that for molecules possessing an asymmetric polarizability tensor. This is illustrated in Table I which lists the size of the DC Kerr effect for some typical symmetric and asymmetric molecules in terms of the parameter B_o,

$$B_o = \frac{\delta n_{//} - \delta n_{\perp}}{\lambda E_o^2}$$

which is called the Kerr constant. Here $\overline{E_o^2}$ is the time average of the square of the strong DC or AC field and λ is the vacuum wavelength of the "test" beam experiencing an index change. We have pointed out previously that the probable origin of the Kerr effect in symmetric-molecule liquids is the spatial "redistribution" or "rearrangement" of the molecules under the influence of the anisotropic dipole-dipole forces induced by a strong applied electric field.[3] However, we have previously attempted to calculate only the magnitude of the quickly responding parallel change in index $\delta n_{//}$ on this hypothesis,[3] rather than the much more easily measured difference $\delta n_{//} - \delta n_{\perp}$ (i.e., Kerr effect).

In these lectures we will discuss the physical basis of molecular redistribution and why it is likely to dominate other effects which might also contribute to the Kerr effect in all but a few symmetric-molecule liquids (Section II). We then develop general expressions for $\delta n_{//}$ and $\delta n_{\perp}$ in terms of configuration averages in the (zero field) equilibrium ensemble of molecules (Section III) and discover that the result depends mainly on the equal-time joint probabilities for two, three and four particles to be in various close configurations. The Kerr effect is probably the most sensitive of all easily measured properties of a fluid of symmetric molecules to this statistical aspect of short range order From the derived expressions we show that, independently of the nature of these correlation functions, the ratio $\delta n_{//} / \delta n_{\perp}$ is nearly -2 for pure molecular redistribution of symmetric molecules (Section IV). It was exactly -2 in the old theories for asymmetric

molecules undergoing no redistribution.[2] Although we find that the ratio is not -2 in general, we show that in any normal liquid the ratio will probably be close enough to -2 so that one may infer the value of the fast responding part of the nonlinear index $\delta n_{//}$ (which generally governs the optical self-focussing properties of the liquid) from DC Kerr constant measurements, to within about 20%. This is important since other ways of measuring $\delta n_{//}$ this accurately are much more difficult. Finally we shall outline how Kirkwood's "superposition approximation" may be used to evaluate the required averages. We find that the result of this calculation gives the wrong sign for B_o at densities about roughly half liquid density (Section V). The results are given for molecules of assymmetric polarizability but symmetric (unperturbed) intermolecular forces, and are seen to reduce to the results of Debye and others in the low density limit.[4] Unfortunately, there is, at present, no way known to calculate the required configurational averages for liquids in a self-consistent manner.

II. ORIGIN OF KERR EFFECT IN SYMMETRIC-MOLECULE FLUIDS

On the basis of evidence available to date, it would appear that symmetric-molecule liquids, such as those of Table I, whose polarizabilities are well in excess of 10^{-24} cm^3 owe their Kerr effect mainly to molecular redistribution. Therefore the remaining parts of these lectures will be devoted to a study of this mechanism. However, for liquids such as of helium and neon whose atoms have low polarizabilities the Kerr effect will probably be mainly due to the electronic nonlinearity of the atoms. The evidence is briefly as follows.

Stuart and Volkmann observed that upon increasing the temperature of liquid CCl_4 14% (to 339°K) the Kerr constant dropped 10%.[5] This behavior is inconsistent with electronic nonlinearities being dominant and is consistent with what is known from redistribution theory. On the other hand, Boyle, et. al., have measured the Kerr constant of helium gas and found it to be proportional to the density as would be expected if electronic nonlinearities were dominant. They[6] and Langhoff, et. al.,[7] have also calculated values for the electronic nonlinearity of helium and predicted values close to each other and to that inferred from the Kerr measurements. The theory of molecular redistribution, which is expected to be accurate at the densities of gas employed in the experiments, predicts a nonlinearity that would be much smaller than that observed and also vary as the square

of the density.[3] Langhoff, et. al., also calculated the nonlinear polarizabilities for many S-state atoms and ions in addition to helium. From their results and a crude extrapolation of redistribution effects to liquid densities, we expect (1) that the Kerr effects in liquid neon would also be electronic, (2) that in liquid argon both electronic and redistribution effects might be observed, and (3) that in more polarizable liquids redistribution is likely to dominate. For example, if we use the calculated nonlinear polarizabilities of the C^{+4} and Cl^{-} ions[7] to calculate the electronic contribution to the Kerr constant B_0 of $C Cl_4$ we obtain a value two orders of magnitude lower than what is observed (and, of course, do not predict the observed temperature dependence of B_0).

There are other mechanisms which contribute to the B_0 of liquids, but they generally contribute a negligible amount. The naturally existing different isotopes of Cl and Br would cause some XCl_4 or YBr_4 type molecules to be slightly asymmetric. This asymmetry can be estimated from the isotopic shifts in spectral lines and appears to contribute negligibly to B_0. This is not surprising in view of the fact that a molecule like cyclohexane whose polarizability and number density in liquid are very close to those of $C Cl_4$ (+4% and -10% respectively), but whose assymmetry is quite large, can nonetheless exhibit a lower Kerr constant than $C Cl_4$.

Similarly, the electronic asymmetry of those molecules that happen to be thermally excited to asymmetric vibrational states can be estimated and is not nearly large enough to account for observed B_0 values or their temperature dependence.

Also, if the light whose index change is being measured has a frequency within ~ 100 Raman (or Brillouin) linewidths from the frequency of the strong Kerr field, then the dispersion from the wing of the Raman line may affect the Kerr constant. This "Raman wing" will never significantly affect "DC" Kerr constants but could contribute to "AC" Kerr constants and might, in particular, add significantly to the nonlinear index seen by a single monochromatic wave. Since this complication is easy to avoid in Kerr measurements, and is easy to calculate if important, we will not consider it further here. We proceed next to calculate the Kerr constant of a fluid, supposing that molecular redistribution were the only mechanism.

III. RELATION BETWEEN A KERR CONSTANT DUE TO MOLECULAR REDISTRIBUTION AND SHORT RANGE ORDER OF A FLUID

Each possible way of arranging N molecules inside a volume V will have a certain probability of existing (given by statistical mechanics) and will exhibit a certain wave of polarization density $P_i \exp(i\underset{\sim}{k} \cdot \underset{\sim}{x} - i\omega t)$ in the presence of a propagating electromagnetic wave $E_j \exp(i\underset{\sim}{k} \cdot \underset{\sim}{x} - i\omega t)$.[2] We assume that each molecule has a real polarizability α that is strictly linear and isotropic at the frequency ω so that the complex amplitude m_i^γ of i.th spatial component of the dipole moment of the γ th molecule is given by[2]

$$m_i^\gamma = \alpha E_i^\gamma . \tag{1}$$

The local electric field amplitude E_i^γ at the position $\underset{\sim}{x}^\gamma$ of the γth molecule consists of the transverse propagating electric field plus a longitudinal (Coulomb) field due to the dipole moments of all the other molecules:

$$E_i^\gamma = E_i e^{i\underset{\sim}{k} \cdot \underset{\sim}{x}^\gamma} - \Sigma_\beta D_{ij}^{\gamma\beta} m_j^\beta , \tag{2}$$

where

$$D_{ij}^{\gamma\beta} \equiv \delta_{ij} |\underset{\sim}{x}^{\gamma} - \underset{\sim}{x}^{\beta}|^{-3} - 3(x_i^{\gamma} - x_i^{\beta})(x_j^{\gamma} - x_j^{\beta}) |\underset{\sim}{x}^{\gamma} - \underset{\sim}{x}^{\beta}|^{-5} \qquad (3)$$

is the usual dipole-dipole matrix. For any given configuration $\{\underset{\sim}{x}^{\gamma}\}$ of molecules, (1) and (2) yield[9]

$$m_i^{\gamma} = \alpha X_{ij}^{\gamma\beta} E_j e^{i\underset{\sim}{k} \cdot \underset{\sim}{x}^{\beta}} \qquad (4)$$

where the $3N \times 3N$ matrix $X_{ij}^{\gamma\beta}$ is defined through its inverse

$$(X^{-1})_{ij}^{\gamma\beta} = \delta_{ij}\delta^{\gamma\beta} + \alpha D_{ij}^{\gamma\beta}. \qquad (5)$$

The polarization density amplitude P_i for the $(\underset{\sim}{k}, \omega)$ wave is $V^{-1} \Sigma_{\gamma} m_i^{\gamma} e^{-i\underset{\sim}{k} \cdot \underset{\sim}{x}^{\gamma}}$ and we wish to calculate the average of P_i over all configurations. If we express this average as

$$\langle P_i \rangle = \chi_{ij} E_j \qquad (6)$$

then the susceptibility tensor χ_{ij} is, from (4)

$$\chi_{ij} = \langle T_{ij}(\{\underset{\sim}{x}^{\gamma}\}) \rangle \qquad (7)$$

where[9]

$$T_{ij}(\{\underset{\sim}{x}^{\gamma}\}) = X_{ij}^{\gamma\beta} (\alpha/V) \exp[i\underset{\sim}{k} \cdot (\underset{\sim}{x}^{\gamma} - \underset{\sim}{x}^{\beta})] \qquad (8)$$

and the brackets <> indicate either a quantum or classical statistical mechanical average over configurations $\{\underset{\sim}{x}^{\gamma}\}$ as is appropriate. The average χ_{ij} of (7) will be generally a function of the existing electric fields because the intermolecular induced-dipole-induced-dipole interaction energy v will affect the weighting function used in the averaging. Given χ_{ij} it is a trivial matter to find the indices of refraction or dielectric tensor of the liquid.

If there exists a strong electric field $E_i' e^{i(\underset{\sim}{k}' \cdot \underset{\sim}{x} - \omega' t)}$ in the fluid, whose frequency ω' and the difference $|\omega' - \omega|$ are large compared to any intermolecular collision rates, then the time average of the induced electronic dipole-dipole interaction energy is[9]

$$v = -\frac{1}{4} V E_i' E_j'^{*} T_{ij}'(\{\underset{\sim}{x}^{\gamma}\}) \qquad (9)$$

for any configuration $\{\underset{\sim}{x}^{\gamma}\}$.[3] The prime on T_{ij}' indicates that it is the same operator as in (8) but with α everywhere replaced by the real polarizability α' at frequency ω' and $\underset{\sim}{k}$ replaced by $\underset{\sim}{k}'$.

We will consider here only classical fluids. Then the average $\langle A(\{\underset{\sim}{x}^{\gamma}\})\rangle$ of some operator A is

$$\{\int d\underset{\sim}{x}^1 \cdots d\underset{\sim}{x}^N A e^{-\frac{v+v_o}{kT}}\} / \{\int d\underset{\sim}{x}^1 \cdots d\underset{\sim}{x}^N e^{-\frac{v+v_o}{kT}}\},$$

and χ_{ij} may be expanded in v/kT to give an expression exact to second order in E':

$$\chi_{ij} = \langle T_{ij} \rangle_o + \chi_{ijlm} E_l' E_m'^* \qquad (10)$$

where[9,10]

$$\chi_{ijlm} = \frac{V}{4kT} (\langle T_{ij} T_{lm}' \rangle_o - \langle T_{ij} \rangle_o \langle T_{lm}' \rangle_o). \qquad (11)$$

The average $\langle \rangle_o$ indicates the average over the unperturbed configurations, where only the unperturbed intermolecular potential v_o acts.

For small $\underset{\sim}{k}$ and $\underset{\sim}{k}'$, χ_{ijlm} cannot depend on $\underset{\sim}{k}$ or $\underset{\sim}{k}'$. Therefore the rotational symmetry of the fluid applied to (11) with (8) will require

$$\chi_{ijlm} \rightarrow \chi_{jilm} \rightarrow \chi_{ijml} \rightarrow \chi_{jiml} \qquad (12)$$

or

$$\chi_{ijlm} \rightarrow A\delta_{ij}\delta_{lm} + B(\delta_{il}\delta_{jm} + \delta_{im}\delta_{jl}) \qquad (13)$$

as $\underset{\sim}{k}, \underset{\sim}{k}' \rightarrow 0$, and the two coefficients A and B determine χ_{ijlm}.

The operator T_{ij} is too difficult to evaluate exactly for an arbitrary distribution; we may proceed to approximate the required averages in any of several ways, all of which yield the same result to lowest order in α. We could, for example, use the fact that v may be expressed as a minimum of a certain expression and minimize an approximate expression with respect to some parameters.[3] Here we will follow the program used by Kirkwood and Yvon to calculate corrections to the Lorentz-Lorenz formula for the linear dielectric constant of a liquid.[11] The RHS of (5) is rewritten as $\delta_{ij}\delta^{\gamma\beta}(1 - \xi) + \phi_{ij}^{\gamma\beta}$ where $\phi_{ij}^{\gamma\beta} \equiv \xi\delta_{ij}\delta^{\gamma\beta} + \alpha D_{ij}^{\gamma\beta}$, and then $X_{ij}^{\gamma\beta}$ is expanded

in powers of $\phi_{ij}^{\gamma\beta}/(1-\xi)$. The parameter ξ is then adjusted to be

$$\xi = 4\pi N\alpha/(3V) \tag{14}$$

so that the first term in the expansion contributes nothing at small k to the transverse part of the linear susceptibility. The hope that this produces a rapidly converging series expansion is born out by the high accuracy (~ 1 to 5%) of the Lorentz-Lorenz formula that then results from the $\phi_{ij}^{\gamma\beta} = 0$ approximation.[11] Expanding (11) to the lowest nonvanishing order gives ($\rho = N/V$ is the average density)

$$\chi_{ijlm} \approx \frac{\rho\alpha\alpha'}{4kT(1-\xi)^2(1-\xi')^2}\sum_{\beta\nu\mu}(\langle C_{ij}^{\gamma\beta}C'_{lm}{}^{\nu\mu}\rangle_o - \langle C_{ij}^{\gamma\beta}\rangle_o\langle C'_{lm}{}^{\nu\mu}\rangle_o) \tag{15}$$

where

$$C_{ij}^{\gamma\beta} = D_{ij}^{\gamma\beta}\exp i\underset{\sim}{k}\cdot(\underset{\sim}{x}^{\gamma} - \underset{\sim}{x}^{\beta}) \tag{16}$$

and similarly for $C'_{lm}{}^{\nu\mu}$ but with $\underset{\sim}{k}$ replaced by $\underset{\sim}{k}'$. The next corrections are of order ξ, ξ' and $\rho\tau$ smaller, where $\tau/8$ is the molecular volume. Judging from the accuracy of the linear term, we feel that, if evaluated exactly, (15) would give the nonlinear part of the index to within 10% for typical liquids.

IV. $\delta n_{//} / \delta n_{\perp}$

The most simple and accurate measurements to perform in practice are of the Kerr constant B_o, i.e., of $\delta n_{//} - \delta n_{\perp}$. However, one desires the value of $\delta n_{//}$ alone for calculating many nonlinear propagation characteristics such as the self-focussing of laser light. It is therefore useful to note that to within the accuracy of the approximation (15) one can calculate the ratio $R = \delta n_{//} / \delta n_{\perp}$, and hence derive $\delta n_{//}$ from B_o (in the long wavelength limit), without knowing how to perform the required averages. We know that (15) must give a result of the form (13) as $k \to 0$. But $\Sigma_i C_{ii}^{\gamma\beta} = \Sigma_i D_{ii}^{\gamma\beta} = \Sigma_i C'_{ii}{}^{\nu\mu} \equiv 0$ so that multiplying both (15) and (13) by $\delta_{ij}\delta_{lm}$ and summing over all space indices gives

$$9A + 6B \approx 0. \tag{17}$$

If the strong electric field E_i' is applied in the x-direction (i = x) then

$$R \equiv \delta n_{//} / \delta n_{\perp} = \chi_{xxxx}/\chi_{yyxx} = (A + 2B)/A \tag{18}$$

so that (17) implies

$$R \approx -2. \tag{19}$$

If we had kept higher order terms in the expansion of the exact expression (11), A would not be exactly - 2 B/3 nor would R be -2. But one might expect that R is -2 to within 10 or 20% for even the densest, most polarizable symmetric-molecule liquids. We will see from the discussion of the next Section that if both reorientation and redistribution are effective, A is not precisely - 2 B/3, even in lowest order. However, again it is close enough so that, even for asymmetric molecules, R would never be likely to deviate from - 2 more than 10 or 20%. It is well known that when only reorientation is important in calculating χ_{ijlm}, R is exactly -2; this is the famous "Langevin relation".[2] That R should be - 2 when $k \to 0$ implies that the trace of χ_{ij} is unchanged by the application of the strong field. It is evident that this should be true when there is only the reorientation of molecules whose polarizability tensor, as viewed from molecular axes, remains unchanged.

V. EVALUATION OF χ_{ijlm} WITH THE KIRKWOOD SUPERPOSITION APPROXIMATION

The only way known to modern statistical mechanics for estimating the averages in the approximate expression (15) for χ_{ijlm} is to use the Kirkwood "superposition" approximation for the two-, three- and four-particle correlation functions required there. That is, one must take the probability $p_4(1234)$ of finding four specific particles at the positions $\underset{\sim}{r}^1$, $\underset{\sim}{r}^2$, $\underset{\sim}{r}^3$ and $\underset{\sim}{r}^4$ (per fraction of the total volume V at each point) as a product

$$p_4(1234) = p(12)\, p(13)\, p(34)\, p(23)\, p(24)\, p(34) \,/\, Q \qquad (20)$$

over all possible pairs of some two particle function p. Then the three- and two-particle correlation functions are determined by the identities

$$p_3(123) = \int p_4(1234)\, d\underset{\sim}{r}^4 / V \qquad (21)$$

and

$$p_2(12) = \int p_3(123)\, d\underset{\sim}{r}^3 / V \qquad (22)$$

respectively. The normalization factor Q ensures that

$$\int p_2(12)\, d\underset{\sim}{r}^1\, d\underset{\sim}{r}^2\, V^{-2} = 1.$$

The only known function p for which dipole averages can be carried out analytically is the simple step function of the absolute value r of the distance between the two space points:

$$p(r) = 1,\ r \geq a_o$$
$$= 0,\ r < a_o \tag{23}$$

whence

$$Q = 1 - 6\tau/N \tag{24}$$

in the limit of large N; $\tau = 4\pi a_o^3/3$ is eight times the volume of our spherical molecules.

We have evaluated the averages required in (15) using the above correlation functions. We have also carried through the averages under all the same assumptions except that the molecular polarizabilities are tensors α_{ij}^{γ} (and $\alpha'_{ij}{}^{\gamma}$) that depend on the orientation of the γth molecule. This means that $\Sigma_k \alpha_{ik}^{\gamma} D_{kj}^{\gamma\beta}$ replaces $\alpha D_{ij}^{\gamma\beta}$ in the definition (5) for $X_{ij}^{\gamma\beta}$, and $\Sigma_k X_{ik}^{\gamma\beta}\alpha_{kj}^{\beta}$ replaces $X_{ij}^{\gamma\beta}\alpha$ in T_{ij} and the interaction energy of (9). The average polarizabilities are still called α and α' and the "best" ξ, ξ' parameters are still $4\pi\rho\alpha/3$ and $4\pi\rho\alpha'/3$.

Also, statistical averages must now include the appropriately normalized integrals over all orientations of all molecules. We do not however change the unperturbed distribution functions (20) - (23) to reflect any molecular asymmetry. The details of

the integration techniques and the organization of the many terms which arise are given in reference (3). The results for the A and B coefficients of (13), with the form of (15) extended as above, are (with the small term K_4 noted in ref. 3 omitted)

$$A = \frac{\rho a a'}{4kT(1-\xi)^2(1-\xi')^2}\left\{\Delta\left(6\xi'\xi - \frac{1}{2}\right)\right.$$

$$\left. - \frac{1}{2}\left[\frac{(\Delta-1)8\pi^2\rho^2 a a'}{3} + 4.51\, a a' \rho^3 \tau + \frac{128\pi^2 \rho a a'}{45\tau}\left(1 - \frac{13}{4}\Delta + \frac{31}{16}\Delta^2\right)\right]\right\} \tag{25a}$$

and

$$B = \frac{\rho a a'}{4kT(1-\xi)^2(1-\xi')^2}\left\{\Delta\left(\frac{3}{4} - 3\xi\xi'\right)\right.$$

$$\left. + \frac{3}{4}\left[\frac{(\Delta-1)8\pi^2\rho^2 a a'}{3} + 4.51\, a a' \rho^3 \tau + \frac{128\pi^2 \rho a a'}{45\tau}\left(1 + \frac{7}{4}\Delta + \frac{33}{8}\Delta^2\right)\right]\right\}. \tag{25b}$$

The dimensionless anisotropy parameter Δ is, as usual,

$$\Delta = \frac{2}{45}\left[\frac{(a-b)(a'-b') + (b-c)(b'-c') + (c-a)(c'-a')}{a a'}\right] \tag{26}$$

where a, b, c, and a', b', c' are the polarizabilities at frequency ω and ω' respectively along the principle axes of the molecules' polarizability tensor. The A and B for purely symmetric molecules come from (25) by putting $\Delta = 0$.

First we note that (25) gives the nonlinear index coefficient n_2 we have calculated previously using the same Kirkwood approximation[3]. From its definition,

$$n_2 = 4\pi\chi_{xxxx}'/n = 4\pi(A+2B)/n \qquad (27)$$

where all primes have been dropped and n is the linear index of refraction at the one frequency ω where the nonlinear index is now self-induced.

Secondly, we note that in the limit of low densities, only the "Δ" terms remain and we have the classical result of Debye and others[4] for the Kerr constant B and the nonlinear index n_2 that arises from molecular re-orientation alone.

However, most important, for α near α', χ_{xxxx} becomes negative for $\rho\tau > 1.6$. For liquid densities $\rho\tau$ runs between 2 and 3. Since χ_{xxxx} is of the form $\langle T_{xx}^2\rangle_o - \langle T_{xx}\rangle_o^2$ when $\alpha = \alpha'$, we see that χ_{xxxx} and n_2 ought always to be positive, and hence the Kirkwood approximation is breaking down entirely at liquid densities. Other failures of this approximation have been found and are noted in the Erratum of reference (3).

The formulae (25) give a maximum positive value for n_2 and B_o (at $\rho\tau \approx 0.32$) which is typically 1/5 of that actually observed in symmetric molecules at liquid densities. We see therefore that at low densities, before (23) fails, the calculation is giving results consistent with what one might expect from measurements on liquids.

Unfortunately, measurements of B_o of symmetric molecules of high polarizability at gas densities where (25) should be accurate have not been made.

In summary, it appears that molecular redistribution is the main cause of the Kerr constant of liquids of symmetric molecules whose polarizabilities are much larger than 10^{-24} cm^3. Experiments at different densities and temperatures will be able to isolate the contribution of molecular redistribution to the Kerr constant of gases. At densities lower than about 1/5 liquid density (25) should give this contribution accurately. Since this contribution depends only on the short range order in the fluid, and is the most sensitive of easily measured properties to the short range order, future theories of the short range order (particularly of the function $p_4(1234)$) may be readily verified by Kerr measurements.

TABLE I

Some values of the Kerr constant B_o for nonpolar liquids, in units of B_b, the Kerr constant of benzene.

$B_b = 4.1 \times 10^{-9}$ esu for $\lambda = 546$ mμ.

Liquid	B_o/B_b
CS_2	8.6
Benzene	1
$Sn Cl_4$ [a]	0.50 [b]
$Si Br_4$ [a]	0.43 [b]
$C Cl_4$ [a]	0.20 [b]
N_2	0.19
Cyclohexane	0.14

[a] Symmetric molecules

[b] These values are from recent measurements of N. George and C. Cook (unpublished).

FOOTNOTES AND REFERENCES

1. J. Kerr, Phil. Mag. [4], 50, 337 (1875).
2. P. Langevin, Le Radium 1, 249 (1910); J. Larmor, Phil. Trans. A, 190 (1898); A. Cotton and H. Mouton, Journ. de phys. (5) 1, 5 (1911); Ann. Chim. Phys. 19, 153 (1910); 20, 194 (1910).
3. R. W. Hellwarth, Phys. Rev. 152, 156 (1966).
4. P. Debye, Marx's Handbuch der Radiologie VI, (Leipzig, 1925); Chap. V, p. 768. This excellent review of the Kerr effect seems to contain the first account of the standard reorientation theory with all the numerical factors and local field corrections treated carefully.
5. H. A. Stuart and M. Volkmann, Z. Physik 83, 444 (1933).
6. L. L. Boyle, A. D. Buckingham, R. L. Disch, and D. A. Dunmur, J. Chem. Phys. 45, 1318 (1966).
7. P. W. Langhoff, J. D. Lyons, and R. P. Hurst, Phys. Rev. 148, 18 (1966).
8. Roman subscripts i, j, ... etc. always denote Cartesian space indices x, y, z. Greek superscripts α, β, ..., etc. are used to label molecules and take the values 1 to N.
9. Repeated space (Roman subscript) and molecule (Greek superscript) indices are to be summed.

10. S. Kielich, Acta Physica Polonica XXXI, 689 (1967), has recently derived a formula for the Kerr constant of a liquid of symmetric molecules (his eq. (5.13)) which claims to include the effects of molecular redistribution; however, it differs markedly from (11) because the intermolecular interaction energy v that is employed is not that of (9). If one used the v of Kielich to compute the free energy f for one wave, one would not obtain the relation $P_i = -4V^{-1}\partial f/\partial E_i^*$ that is the correct extension of the more familiar relation $M_i^o = -\partial f/\partial E_i^o$ for the static moment M_i^o of a sample in a static external field E_i^o.

11. See C. J. F. Böttcher, Theory of Electric Polarization (Elsevier Publishing Co., Amsterdam, 1952) for a review of such corrections and references.